Semi-implicit-linearized multiple-relaxation-time formulation of lattice Boltzmann schemes for mixture modeling

Pietro Asinari
Department of Energetics, Politecnico di Torino, Corso Duca degli Abruzzi 24, Torino, Italy
(Received 19 December 2005; revised manuscript received 9 March 2006; published 22 May 2006)

A lattice Boltzmann model for mixture modeling is developed by applying the multiple-relaxation-time (MRT) approach to the Hamel model, which allows one to derive from a general framework different model equations independently proposed, like the Gross-Krook model and the Sirovich model. By imposing some physical constraints, the MRT lattice-Boltzmann Hamel model reduces to the generalized MRT lattice-Boltzmann Gross-Krook model (involving the local Maxwellian centered on the barycentric velocity), which allows one to tune independently the species diffusivity, the mixture kinematic viscosity, and the mixture bulk viscosity. Reducing the number of moving particles over the total is possible to deal effectively with mass particle ratios far from unity and, for this reason, to model the pressure-driven diffusion. A convenient numerical approach is proposed for solving the developed model, which essentially widens the stability range of conventional schemes in terms of dimensionless relaxation frequencies, by solving explicitly the advection operator together with the nonlinear terms of the collisional operator and solving implicitly the residual linear terms. In this way, the calculations are drastically reduced and the operative matrices can be computed once for all, at the beginning of the calculation (implying moderate additional computational demand). Following this approach, a semi-implicit-linearized backward Euler scheme, ideal for parallel implementations, is proposed. In order to achieve the previous results, the asymptotic analysis, recently suggested for analyzing the macroscopic equations corresponding to lattice-Boltzmann schemes in the low-Mach-number limit, proves to be an effective tool. Some numerical tests are reported for proving the consistency of the proposed method with both the Fick model and Maxwell-Stefan model in the macroscopic limit.

DOI: 10.1103/PhysRevE.73.056705 PACS number(s): 47.11.−j, 47.10.−g, 51.10.+y

I. INTRODUCTION

In the last years, the lattice Boltzmann method (LBM) has become very popular among the discretization techniques for solving simplified kinetic models. Starting from some pioneer works [1–3], the method has reached a more systematic fashion [4,5] by means of a better understanding of the connections with the continuous kinetic theory [6,7] and by widening the set of applications, which can benefit from this numerical technique. When complex geometries are considered and interparticle interactions must be taken into account, the discretized models derived by means of the lattice Boltzmann method offer some computational advantages over continuum-based models, particularly for large parallel computing. In order to appreciate the connection between the lattice Boltzmann method and conventional finite-difference techniques, it is useful to recognize that this method can be considered a useful subclass of fully Lagrangian methods [8]. A more complete and recent coverage of various previous contributions to the LBM is beyond the purposes of the present paper, but can be found in some books [9–11] and some review papers [12,13].

A promising application for lattice Boltzmann models seems to be the analysis of reactive mixtures in porous catalysts [14,15]. For this reason, a lot of work has been performed in recent years in order to produce reliable lattice Boltzmann models for multicomponent fluids and, in particular, for mixtures composed by miscible species. The problem is to find a proper way, within the framework of a simplified kinetic model, for describing the interactions among particles of different types—i.e., cross collisions. Once this milestone is defined, the extension of the model to reactive flows is straightforward [16,17] and it essentially involves additional source terms in the species equations according to the reaction rate.

Unfortunately, most existing lattice Boltzmann models for mixtures are based on pseudopotential interactions [18–21] or heuristic free energies [22–25] in order to realize the so-called *single-fluid approach* [26,27]. Essentially, the averaged effect due to both self-collisions and cross collisions is described by means of a total Bhatnagar-Gross-Krook-like (BGK-like) collisional operator. Considering some special kind of mixture properties in the Maxwellian distribution function of the BGK-like collisional operator, each species will be forced to evolve towards the mixture equilibrium conditions. For almost a decade now, diffusions driven by concentrations, pressure, temperature, and external forces have been studied by this kind of models for an arbitrary number of components with nonideal interactions. Even though the single-fluid approach proved to be an accurate numerical tool for solving some macroscopic equations in a large number of applications, it provides a mesoscopic picture of the phenomena which shows some limits (see the next section for details).

On the other hand, some models based on the *multiple-fluid approach* have been proposed. According to this approach, each species relaxes towards its equilibrium configuration according to its specific relaxation time constants and some coupling must be considered in order to describe the collisions among different species. Some models [28,29] adopt a *force coupling* in the momentum equations, which derives from a linearized kinetic term, while other models

[30,31] avoid any linearization of the coupling effect.

In particular, the Hamel model [32–34], originally developed as a simplified kinetic equation for mixture modeling, allows one to derive from a general framework different model equations independently proposed, like the Gross-Krook model [35] and the Sirovich model [36], which are the theoretical forerunners of the single-fluid and multiple-fluid approaches, respectively. For this reason, the Hamel model allows one to describe mixtures at different limiting regimes consistently. An LB discrete formulation of the continuous kinetic model proposed by Hamel has been recently proposed [31].

The goals of this paper are the following: (i) To extend the previous LB formulation of the Hamel model by means of the multiple-relaxation-time [37,38] (MRT) approach in order to independently tune the macroscopic transport coefficients and to clarify once for all how the Hamel model is related to the other conventional models (in particular the Gross- Krook model and the Sirovich model); (ii) to find a simple way for modeling the additional effects due to pressure diffusivity when mass particle ratios far from unit are considered; (iii) to identify the best numerical scheme for mixture modeling in terms of accuracy, stability, and simplicity for dealing with parallel implementation; (iv) finally to test the suitability for the considered application of the asymptotic analysis [39,40], recently suggested as an effective tool for analyzing the macroscopic equations corresponding to LB schemes.

This paper is organized as follows.

Section II A clarifies some general issues concerning the single-fluid and multiple-fluid approaches. Section II B summarizes the previous single-relaxation-time formulation of the Hamel model by introducing a new compact form. Section II B generalizes the previous formulation by means of the multiple-relaxation-time approach for the continuous case.

Section III A shows some limits of the Chapman-Enskog expansion for the considered model. Section III B recovers the macroscopic equations which correspond to the continuous model by means of the asymptotic analysis.

Section IV A introduces the proposed semi-implicit-linearized (SIL) approach. Section IV B discusses the memory-optimized (single-step) integration formulas, while Sec. IV C discusses the speed-optimized (multiple-step) integration formulas. Section IV D introduces the proposed semi-implicit-linearized backward-Euler (SILBE) formula, which is analyzed by means of the asymptotic analysis in the Sec. IV E.

In Sec. V A the stability analysis by means of the eigenvalue spectra for single-step integration formulas is reported. Section V B reports the numerical results concerning the decay of the sine-wave density profile. Section V C discusses the numerical results for the Taylor-Green vortex flow. Finally, Sec. V D deals with some numerical tests, purposely developed for proving the consistency of the proposed method with both the Fick model and Maxwell-Stefan model in the macroscopic limit.

Section VI summarizes the conclusions of this work.

II. LATTICE BOLTZMANN MODELS FOR MIXTURES

A. Single-fluid versus multi-fluid approach

Before proceeding with the discussion of the lattice Boltzmann models for mixtures and how to integrate them numerically, it is worth the effort to clarify some basic concepts regarding the dichotomy between *single-fluid* and *multiple-fluid* approaches.

In the framework of the lattice Boltzmann method, the set of microscopic velocities is so small that a proper model Boltzmann equation—i.e., a simplified collision operator—must be considered in order to describe the time dynamics of the distribution function due to collisions. Unfortunately there is considerably more latitude in the choice of a linearization procedure in the case of a mixture than for a pure gas [41]. In the latter case, a local Maxwellian centered on the (uniquely defined) macroscopic velocity is usually a candidate for the unperturbed component of the distribution function. In a mixture, however, it is possible to linearize about a local Maxwellian which contains the barycentric velocity or, alternatively, we can introduce distinct species flow velocities and linearize about local Maxwellians which contain these quantities.

The theory of the collision operators which results in the latter case is complicated by the fact that these operators will not have the usual symmetry properties. In particular the leading term—i.e., the unperturbed term—of the distribution function could be no longer Maxwellian and, for this reason, the application of the usual expansion technique based on this assumption, like the Chapman-Enskog procedure, could be doubtful at least. On the other hand, when one species is considerably heavier than the other, or present at considerably higher concentration, then self-collisions tend to play a dominant role, so that the species first equilibrate individually and only then mutually [41]. Even though it could yield to slightly more complicated models, the choice of separate Maxwellians seems more general and better suited for dealing with different regimes consistently.

For this reason, the Hamel model [32–34] seems very promising for mixture modeling by the lattice Boltzmann method, because it makes use of collision operators involving both the Maxwellian centered on the barycentric velocity and those centered on the distinct species flow velocities. According to this model, the distribution function g_σ for the generic species σ satisfies the following equation:

$$\frac{\partial g_\sigma}{\partial t} + \mathbf{v} \cdot \nabla g_\sigma = \frac{1}{\tau_\sigma}(g_\sigma^e - g_\sigma) + \frac{1}{\tau_m}(g^e - g_\sigma), \tag{1}$$

where $g_\sigma^e = g_*^e(\mathbf{u}_\sigma)$, $g_{\sigma m}^e = g_*^e(\mathbf{u})$, and $g_*^e(\mathbf{u}_*)$ is defined as

$$g_*^e(\mathbf{u}_*) = \frac{\rho_\sigma}{m_\sigma (2\pi e_\sigma)^{D/2}} \exp\left[-\frac{(\mathbf{v} - \mathbf{u}_*)^2}{2e_\sigma} \right]. \tag{2}$$

In particular $\mathbf{u}_\sigma$ is the single-species velocity and $\mathbf{u}$ is the barycentric velocity, defined as the mass average of the single-species velocities—i.e., $\mathbf{u} = \Sigma_\sigma x_\sigma \mathbf{u}_\sigma$ where x_σ is the generic mass concentration.

If both collision operators are considered, then the linearized model can be defined consistent with the *multiple-fluid*

approach and, in this case, the relaxation time constants τ_σ and τ_m can be tuned for modeling the equilibration processes due to self-collisions and cross collisions, respectively. On the other hand, if $1/\tau_\sigma=0$, then the model reduces to the structure prescribed by the *single-fluid* approach and the residual relaxation time constant τ_m can be tuned for modeling the mutual effects due to both self-collisions and cross collisions.

Independently of the considered choice, all the models must ensure the macroscopic continuity equation for the distinct species (and consequently for the mixture), the macroscopic momentum equation for the barycentric velocity, and the diffusive law as the leading term of the distinct species momentum—namely,

$$\frac{\partial \rho_\sigma}{\partial t} + \nabla \cdot (\rho_\sigma \mathbf{u}_\sigma) = 0, \tag{3}$$

$$\frac{\partial}{\partial t}(\rho \mathbf{u}) + \nabla \cdot (\rho \mathbf{u} \otimes \mathbf{u}) = -\nabla p + \nabla[\eta_m \nabla \cdot (\rho \mathbf{u})] + \nabla \cdot [\nu_m \nabla (\rho \mathbf{u}) + \nu_m \nabla (\rho \mathbf{u})^T], \tag{4}$$

$$\rho_\sigma \mathbf{u}_\sigma = \rho_\sigma \mathbf{u} - D_\sigma \nabla \rho_\sigma + O(\mathbf{u}^2). \tag{5}$$

This means that *multiple-fluid* and *single-fluid* approaches could only differ with regards to $O(\mathbf{u}^2)$ terms in the distinct species momentum; namely, they can recover distinct species momentum equations including different $O(\mathbf{u}^2)$ terms. Since summing over the distinct species equations the same equation for the barycentric momentum must be recovered, then these additional terms, which explain the discrepancy between *multiple-fluid* and *single-fluid* approaches, must be linear functions of $(\rho_\sigma - \rho)$ and/or $\rho_\sigma \mathbf{w}_\sigma = \rho_\sigma(\mathbf{u}_\sigma - \mathbf{u})$, because $\Sigma_\sigma(\rho_\sigma - \rho)=0$ and $\Sigma_\sigma \rho_\sigma \mathbf{w}_\sigma = 0$. In the macroscopic modeling, these additional terms, which effect the diffusion law, are usually neglected. For this reason, determining which terms are preferable in order to chose between the *multiple-fluid* and *single-fluid* approaches can only be done by recalling the results due to the continuous kinetic theory.

In the next section, the single-relaxation-time (SRT) formulation of the Hamel model on the D2Q9 lattice will be discussed.

B. Single-relaxation-time formulation of the Hamel model on the D2Q9 lattice

Introducing a proper two-dimensional lattice (D2Q9) for the microscopic velocity and considering the limiting case $U/c \ll 1$, where U is a characteristic macroscopic flow speed and c is the lattice speed, leads to the SRT formulation of the Hamel model [31]—namely,

$$\frac{\partial f^i_\sigma}{\partial t} + \mathbf{v}^i \cdot \nabla f^i_\sigma = \lambda_\sigma (f^{ei}_\sigma - f^i_\sigma) + \lambda_m (f^{ei}_m - f^i_\sigma), \tag{6}$$

where $f^{ei}_\sigma = f^{ei}_\sigma(\mathbf{u}_\sigma)$ is the equilibrium distribution function centered on the species velocity and $f^{ei}_m = f^{ei}_m(\mathbf{u})$ is the equilibrium distribution function centered on the barycentric velocity, defined as the mass average of the species velocities.

It is possible to reformulate the previous equation in a simpler way,

$$\frac{\partial f^i_\sigma}{\partial t} + \mathbf{v}^i \cdot \nabla f^i_\sigma = (\lambda_\sigma + \lambda_m)(f^{ei}_{\sigma m} - f^i_\sigma), \tag{7}$$

where $f^{ei}_{\sigma m} = (1-\alpha_\sigma) f^{ei}_\sigma + \alpha_\sigma f^{ei}_m$ and $\alpha_\sigma = \lambda_m/(\lambda_\sigma + \lambda_m)$. The modified equilibrium distribution function is defined as

$$f^{ei}_{\sigma m} = \rho_\sigma s^i_I \left\{ s^i_0/s^i_I + \frac{3}{c^2}\mathbf{v}^i \cdot [(1-\alpha_\sigma)\mathbf{u}_\sigma + \alpha_\sigma \mathbf{u}] + \frac{9}{2c^4}[(1-\alpha_\sigma) \times (\mathbf{v}^i \cdot \mathbf{u}_\sigma)^2 + \alpha_\sigma (\mathbf{v}^i \cdot \mathbf{u})^2] - \frac{3}{2c^2}[(1-\alpha_\sigma)\mathbf{u}^2_\sigma + \alpha_\sigma \mathbf{u}^2] \right\}, \tag{8}$$

where the weight vectors are

$$\mathbf{s}_0 = (1 - 5/9 s_\sigma), \quad [s_\sigma/9, s_\sigma/9, s_\sigma/9, s_\sigma/9, s_\sigma/36, s_\sigma/36, s_\sigma/36, s_\sigma/36]^T, \tag{9}$$

$$\mathbf{s}_I = [4/9, 1/9, 1/9, 1/9, 1/9, 1/36, 1/36, 1/36, 1/36]^T, \tag{10}$$

and finally $s_\sigma = 3e_\sigma/c^2$. It is easy to prove that if $s_\sigma = 1$, then $\mathbf{s}_0 = \mathbf{s}_I$. The constants in $\mathbf{s}_I$ are the usual weight factors for this lattice [5], and e_σ is the internal energy. The previous equations can be written in vectorial form—namely,

$$\frac{\partial \mathbf{f}_\sigma}{\partial t} + \mathbf{V} \cdot \nabla \mathbf{f}_\sigma = (\lambda_\sigma + \lambda_m)\mathbf{I}(\mathbf{f}^e_{\sigma m} - \mathbf{f}_\sigma), \tag{11}$$

where $\mathbf{V}$ is defined as

$$\mathbf{V}^T = c \begin{bmatrix} 0 & 1 & 0 & -1 & 0 & 1 & -1 & -1 & 1 \\ 0 & 0 & 1 & 0 & -1 & 1 & 1 & -1 & -1 \end{bmatrix}. \tag{12}$$

In the previous equation and in the following of this paper, the dot product between matrices must be thought as saturating the second index: in fact, $\mathbf{V} \in \mathbb{R}^{9\times 2}$, $\nabla \mathbf{f}_\sigma \in \mathbb{R}^{9\times 2}$, and $\mathbf{V} \cdot \nabla \mathbf{f}_\sigma \in \mathbb{R}^9$.

It is possible to consider an equivalent moment system of the previous model by defining a proper set of moments. The lower-order moments are the conserved hydrodynamic moments, but the higher-order nonhydrodynamic moments are unknown. Since the final goal of the moment formulation is to decouple the different moments in order to relax them differently, it is seems natural to consider an orthogonalization procedure: in the following, the well-known Graham-Schmidt procedure will be considered. In order to apply this procedure, two elements are needed: the generalized scalar product and the starting nonorthogonal basis. Concerning the first issue, it has been shown [40] that the scalar product, which includes the weight factors, namely,

$$\langle \mathbf{x}, \mathbf{y} \rangle = (\mathbf{s}_I \oplus \mathbf{x} \oplus \mathbf{y}) = \sum_{i=0}^{8} s^i_I x^i y^i, \tag{13}$$

generates an orthogonal basis clearly separating the terms in the distribution function according to the power of macroscopic velocities. In the previous definition, the generalized

saturation product $\oplus$, defined with regards to the coordinate identifying the lattice components only, has been used. This product can be applied for generating higher-order tensors as well, and the dimension of the result depends on the number of residual indices, once the coordinate identifying the lattice components has been saturated: for examples,

$$\rho_\sigma = \mathbf{1} \oplus \mathbf{f}_\sigma, \quad \rho_\sigma \mathbf{u}_\sigma = \mathbf{V} \oplus \mathbf{f}_\sigma,$$

$$\mathbf{T}_\sigma = \mathbf{V} \oplus \mathbf{V} \oplus \mathbf{f}_\sigma.$$

Concerning the starting nonorthogonal basis, it is essentially a matter of convenience: for simplicity, a simple monomial basis will be considered $\{1, \hat{v}_x, \hat{v}_y, \hat{v}_x\hat{v}_y, \hat{v}_x^2, \hat{v}_y^2, \hat{v}_x\hat{v}_y^2, \hat{v}_y\hat{v}_x^2, \hat{v}_x^2\hat{v}_y^2\}$, where $\hat{v}_x = v_x/c$ and $\hat{v}_y = v_y/c$. These assumptions yield the following linear mapping:

$$\mathbf{M}_A = \begin{bmatrix} 1 & 1 & 1 & 1 & 1 & 1 & 1 & 1 & 1 \\ 0 & 1 & 0 & -1 & 0 & 1 & -1 & -1 & 1 \\ 0 & 0 & 1 & 0 & -1 & 1 & 1 & -1 & -1 \\ 0 & 0 & 0 & 0 & 0 & 1 & -1 & 1 & -1 \\ -1/3 & 2/3 & -1/3 & 2/3 & -1/3 & 2/3 & 2/3 & 2/3 & 2/3 \\ -1/3 & -1/3 & 2/3 & -1/3 & 2/3 & 2/3 & 2/3 & 2/3 & 2/3 \\ 0 & -1 & 0 & 1 & 0 & 2 & -2 & -2 & 2 \\ 0 & 0 & -1 & 0 & 1 & 2 & 2 & -2 & -2 \\ 1 & -2 & -2 & -2 & -2 & 4 & 4 & 4 & 4 \end{bmatrix}, \tag{14}$$

which allows us to define the full set of equilibrium moments for self-collisions,

$$\mathbf{m}_\sigma^e = \mathbf{M}_A \mathbf{f}_\sigma^e = \rho_\sigma [1, \hat{u}_{\sigma x}, \hat{u}_{\sigma y}, \hat{u}_{\sigma x}\hat{u}_{\sigma y}, (s_\sigma - 1)/3 + \hat{u}_{\sigma x}^2, (s_\sigma - 1)/3 + \hat{u}_{\sigma y}^2, 0, 0, 1 - s_\sigma]^T, \tag{15}$$

and cross collisions,

$$\mathbf{m}_m^e = \mathbf{M}_A \mathbf{f}_m^e = \rho_\sigma [1, \hat{u}_x, \hat{u}_y, \hat{u}_x\hat{u}_y, (s_\sigma - 1)/3 + \hat{u}_x^2, (s_\sigma - 1)/3 + \hat{u}_y^2, 0, 0, 1 - s_\sigma]^T. \tag{16}$$

The same mapping $\mathbf{M}_A$ can be used for defining the generic nonequilibrium moments—namely, $\mathbf{m}_\sigma = \mathbf{M}_A \mathbf{f}_\sigma$—which are rescaled by means of the lattice speed in order to ensure that all the moments have the same physical dimensions equal to those of the density. Finally, the equivalent moment system corresponding to Eq. (11) is

$$\frac{\partial \mathbf{m}_\sigma}{\partial t} + \mathbf{M}_A \mathbf{V} \cdot (\mathbf{M}_A^{-1} \boldsymbol{\nabla} \mathbf{m}_\sigma) = (\lambda_\sigma + \lambda_m) \mathbf{I} (\mathbf{m}_{\sigma m}^e - \mathbf{m}_\sigma), \tag{17}$$

where $\mathbf{m}_{\sigma m}^e = (1 - \alpha_\sigma)\mathbf{m}_\sigma^e + \alpha_\sigma \mathbf{m}_m^e$. These preliminary results, which are equivalent to those reported in the paper discussing the SRT formulation of the Hamel model [31], will be generalized in the following section. However, it is worth pointing out that the dichotomy between the *single-fluid* and *multiple-fluid* approaches is reduced by considering a generalized equilibrium distribution function $\mathbf{m}_{\sigma m}^e$, which involves both distinct species and mixture macroscopic properties.

C. Multiple-relaxation-time formulation of the Hamel model on the D2Q9 lattice

The previous vectorial equation (11) can be formally generalized as

$$\frac{\partial \mathbf{f}_\sigma}{\partial t} + \mathbf{V} \cdot \boldsymbol{\nabla} \mathbf{f}_\sigma = \mathbf{A}_\sigma (\mathbf{f}_\sigma^e - \mathbf{f}_\sigma) + \mathbf{A}_m (\mathbf{f}_m^e - \mathbf{f}_\sigma), \tag{18}$$

where $\mathbf{A}_\sigma = \mathbf{M}_D^{-1} \mathbf{D}_\sigma \mathbf{M}_D$, $\mathbf{A}_m = \mathbf{M}_D^{-1} \mathbf{D}_m \mathbf{M}_D$, and $\mathbf{M}_D$ defines a proper orthonormal basis. In particular, $\mathbf{D}_\sigma$ and $\mathbf{D}_m$ are diagonal matrices,

$$\mathrm{diag}(\mathbf{D}_\sigma) = [\lambda_\sigma^0, \lambda_\sigma^I, \lambda_\sigma^I, \lambda_{\sigma 1}^{II}, \lambda_{\sigma 2}^{II}, \lambda_{\sigma 3}^{II}, \lambda_\sigma^{III}, \lambda_\sigma^{III}, \lambda_\sigma^{IV}]^T,$$

$$\mathrm{diag}(\mathbf{D}_m) = [\lambda_m^0, \lambda_m^I, \lambda_m^I, \lambda_{m1}^{II}, \lambda_{m2}^{II}, \lambda_{m3}^{II}, \lambda_m^{III}, \lambda_m^{III}, \lambda_m^{IV}]^T, \tag{19}$$

collecting the generalized relaxation time constants for self-collisions and cross collisions, respectively.

In the equivalent moment space, the previous equation can be reformulated as

$$\frac{\partial \mathbf{m}_\sigma}{\partial t} + \mathbf{M}_A \mathbf{V} \cdot (\mathbf{M}_A^{-1} \boldsymbol{\nabla} \mathbf{m}_\sigma) = \mathbf{E}_\sigma (\mathbf{m}_\sigma^e - \mathbf{m}_\sigma) + \mathbf{E}_m (\mathbf{m}_m^e - \mathbf{m}_\sigma), \tag{20}$$

where $\mathbf{E}_\sigma = \mathbf{M}_A \mathbf{A}_\sigma \mathbf{M}_A^{-1}$ and $\mathbf{E}_m = \mathbf{M}_A \mathbf{A}_m \mathbf{M}_A^{-1}$. The easiest choice is obviously $\mathbf{M}_D = \mathbf{M}_A$, because in this case $\mathbf{E}_\sigma = \mathbf{D}_\sigma$ and $\mathbf{E}_m = \mathbf{D}_m$. The choice of $\mathbf{M}_D$ determines how the macroscopic transport coefficients depend on the relaxation time constants. Even though this arbitrary choice will not alter the number of tunable parameters for a given lattice, it would be desirable to realize a one-to-one direct link between the mac-

roscopic transport coefficients and the relaxation time constants. In particular, the easiest choice will force one to solve a simple linear set of equations in order to tune the relaxation time constants for recovering the desired values of the kinematic and bulk viscosity. For avoiding this additional step, a slightly different choice is adopted and the practical advantages will be discussed by the asymptotic analysis discussed in the next section—namely,

$$\mathbf{M}_D = \begin{bmatrix} 1 & 1 & 1 & 1 & 1 & 1 & 1 & 1 & 1 \\ 0 & 1 & 0 & -1 & 0 & 1 & -1 & -1 & 1 \\ 0 & 0 & 1 & 0 & -1 & 1 & 1 & -1 & -1 \\ 0 & 0 & 0 & 0 & 0 & 1 & -1 & 1 & -1 \\ 0 & 1/2 & -1/2 & 1/2 & -1/2 & 0 & 0 & 0 & 0 \\ -2/3 & -1/6 & -1/6 & -1/6 & -1/6 & 1/3 & 1/3 & 1/3 & 1/3 \\ 0 & -1 & 0 & 1 & 0 & 2 & -2 & -2 & 2 \\ 0 & 0 & -1 & 0 & 1 & 2 & 2 & -2 & -2 \\ 1 & -2 & -2 & -2 & -2 & 4 & 4 & 4 & 4 \end{bmatrix}. \tag{21}$$

In order to reduce the truncation errors, some relaxation time constants will be assumed equal to zero: $\lambda_\sigma^0=\lambda_\sigma^I=0$ because $m_\sigma^{ei}=m_\sigma^i$ for $i=0,1,2$ and $\lambda_m^0=0$ because $m_m^{e0}=m_\sigma^0$ respectively.

As previously done for the SRT formulation, it is possible to search for a more compact form. In particular, let us introduce the matrix $\mathbf{X}_\sigma$, defined as

$$\mathbf{X}_\sigma = \mathbf{M}_A\mathbf{M}_D^{-1}\mathbf{X}_\sigma^0\mathbf{M}_D\mathbf{M}_A^{-1}, \tag{22}$$

where $\mathbf{X}_\sigma^0$ is a diagonal matrix such as

$$\mathrm{diag}(\mathbf{X}_\sigma^0) = [1,1,1,\alpha_{\sigma 1}^{II},\alpha_{\sigma 2}^{II},\alpha_{\sigma 3}^{II},\alpha_\sigma^{III},\alpha_\sigma^{III},\alpha_\sigma^{IV}]^T \tag{23}$$

and $\alpha_{\sigma j}^k=\lambda_{mj}^k/(\lambda_{\sigma j}^k+\lambda_{mj}^k)$. It is possible to prove that the following equivalences hold:

$$\mathbf{E}_\sigma = (\mathbf{E}_\sigma + \mathbf{E}_m)(\mathbf{I}-\mathbf{X}_\sigma), \tag{24}$$

$$\mathbf{E}_m = (\mathbf{E}_\sigma + \mathbf{E}_m)\mathbf{X}_\sigma. \tag{25}$$

Introducing the previous equivalences in Eq. (20) yields

$$\frac{\partial \mathbf{m}_\sigma}{\partial t} + \mathbf{M}_A\mathbf{V}\cdot(\mathbf{M}_A^{-1}\,\boldsymbol{\nabla}\,\mathbf{m}_\sigma) = (\mathbf{E}_\sigma+\mathbf{E}_m)(\mathbf{m}_*^e-\mathbf{m}_\sigma), \tag{26}$$

where $\mathbf{m}_*^e=(\mathbf{I}-\mathbf{X}_\sigma)\mathbf{m}_\sigma^e+\mathbf{X}_\sigma\mathbf{m}_m^e$. Coming back to the discrete velocity space, the compact form becomes

$$\frac{\partial \mathbf{f}_\sigma}{\partial t} + \mathbf{V}\cdot\boldsymbol{\nabla}\mathbf{f}_\sigma = \mathbf{A}_*(\mathbf{f}_*^e-\mathbf{f}_\sigma), \tag{27}$$

where $\mathbf{A}_*=\mathbf{M}_A^{-1}(\mathbf{E}_\sigma+\mathbf{E}_m)\mathbf{M}_A$ and

$$\mathbf{f}_*^e = (\mathbf{I}-\mathbf{M}_D^{-1}\mathbf{X}_\sigma^0\mathbf{M}_D)\mathbf{f}_\sigma^e + \mathbf{M}_D^{-1}\mathbf{X}_\sigma^0\mathbf{M}_D\mathbf{f}_m^e. \tag{28}$$

The matrix $\mathbf{A}_*$ is singular; then, a pseudoinverse must be defined as

$$\mathbf{A}_*^\dagger\mathbf{A}_* = \mathbf{A}_*\mathbf{A}_*^\dagger = \mathbf{I}-\mathbf{Q}, \tag{29}$$

where $\mathbf{Q}=1/9(\mathbf{1}\otimes\mathbf{1})$. This definition differs from that reported Ref. [40], because the kernel of the generalized matrix $\mathbf{A}_*$ is smaller, since the single-species momentum is not conserved (at least for $\lambda_m^I>0$).

In the next section, the asymptotic analysis will be applied in order to recover the macroscopic equations, which derive from the generalized MRT formulation of the Hamel model.

III. CONSISTENCY ANALYSIS

A. Limits of the Chapman-Enskog expansion for the considered model

The compact form given by Eq. (27) allows one to realize that the leading term of the distribution function is $\mathbf{f}_*^e$. Even though this term is a function of macroscopic quantities only, unfortunately it is no longer a local Maxwellian centered on whatever macroscopic velocity. This can be better understood by splitting $\mathbf{f}_*^e$ according to the order of the monomial terms with regards to the macroscopic velocity—i.e., $\mathbf{f}_*^e=\mathbf{f}_*^{e0}+\mathbf{f}_*^{e1}+\mathbf{f}_*^{e2}$. In particular, $\mathbf{f}_*^{ej}=\mathbf{M}_A^{-1}\mathbf{m}_*^{ej}$ and

$$\mathbf{m}_*^{e0} = \rho_\sigma[1,0,0,0,(s_\sigma-1)/3,(s_\sigma-1)/3,0,0,(1-s_\sigma)]^T, \tag{30}$$

$$\mathbf{m}_*^{e1} = \rho_\sigma[0,u_x,u_y,0,0,0,0,0,0]^T, \tag{31}$$

$$\mathbf{m}_*^{e2} = \rho_\sigma \begin{bmatrix} 0 \\ 0 \\ 0 \\ (1-\alpha_{\sigma 1}^{II})u_{\sigma x}u_{\sigma y} + \alpha_{\sigma 1}^{II}u_x u_y \\ (1-\beta_{3p2})u_{\sigma x}^2 - \beta_{3m2}u_{\sigma y}^2 + \beta_{3p2}u_x^2 + \beta_{3m2}u_y^2 \\ -\beta_{3m2}u_{\sigma x}^2 + (1-\beta_{3p2})u_{\sigma y}^2 + \beta_{3m2}u_x^2 + \beta_{3p2}u_y^2 \\ 0 \\ 0 \\ 0 \end{bmatrix}, \tag{32}$$

where $\beta_{3p2}=(\alpha_{\sigma 3}^{II}+\alpha_{\sigma 2}^{II})/2$ and $\beta_{3m2}=(\alpha_{\sigma 3}^{II}-\alpha_{\sigma 2}^{II})/2$.

As far as the monomial terms of $\mathbf{f}_*^e$ with different orders with regards to the macroscopic velocity are independently interpolated, it is evident that this leading distribution cannot be considered a local Maxwellian centered on any macroscopic velocity, deriving from distinct species and mixture velocity. This could be a problem for the basic assumptions underlying the Chapman-Enskog procedure. Interpolating differently the monomial terms with different order will break the usual symmetry properties of the leading expansion coefficient.

First of all, the leading expansion coefficient is expected to be a local Maxwellian by the Chapman-Enskog procedure in order to decouple the equations governing the dynamics of the expansion coefficients. However, as far as mixture modeling is concerned, it is quite easy to force this condition and to derive a generalized Chapman-Enskog procedure, because the residual coupling among the equations governing the dynamics of the expansion coefficients must be proportional to the diffusion velocity and it must produce no effects to the mixture equations [31]. Another way to bypass the problem in a more general fashion is to express the corrections to the leading distribution (whatever it is) by means of the Taylor expansion coefficients [42].

Second, the fact that the Chapman-Enskog procedure does not expand the macroscopic variables but only the distribution function is well known as an intrinsic advantage of this technique in terms of simplicity, as well as an intrinsic limit when compared with more rigorous techniques, like the Hilbert expansion [43]. In particular, for the present application, different macroscopic velocities are involved in the leading distribution function and different interpolating strategies may be considered for each term. For this reason, the hypothesis that different scales governing the macroscopic hydrodynamic invariants are still well separated seems somehow doubtful.

Since in the present paper only diffusion phenomena characterized by slow velocities will be considered, a practicable alternative will be discussed in the next section.

B. Asymptotic analysis of the MRT Hamel model by the diffusive scaling

For most of the diffusion phenomena, the characteristic velocities are usually much smaller than the sound speed. For this reason, the diffusive scaling [44] can be properly applied. In the following, a brief analysis of the general Hamel model by means of the so-called Sone expansion technique will be reported [44].

There are three characteristic time scales in this system: the time scale T_C, which properly describes the collision phenomenon—i.e., $O(\tau_\sigma/T_C)=1$; the time scale T_F, which properly describes the particle dynamics on the lattice—i.e., $O[(L/c)/T_F]=1$ where L is the system size; and, finally, the time scale T_S, which properly describes the slow fluid dynamics—i.e., $O[(L/U)/T_S]=1$. The fast fluid dynamics (acoustic waves) was neglected. Since a lot of collisions are needed in order to travel across the system, then $T_C/T_F=\epsilon$, where ϵ is a small number. Moreover, since $U/c \ll 1$, then $T_F/T_S=\epsilon$ and consequently $T_C/T_S=\epsilon^2$. Once the characteristic time scales are defined, the basic idea is to express the previous equation in terms of some normalized quantities, in order to analyze the slow fluid dynamics only. Applying the diffusive scaling to Eq. (27) yields

$$\epsilon^2 \frac{\partial \mathbf{f}_\sigma}{\partial \hat{t}} + \epsilon \hat{\mathbf{V}} \cdot \hat{\nabla} \mathbf{f}_\sigma = \hat{\mathbf{A}}_* (\mathbf{f}_*^e - \mathbf{f}_\sigma), \tag{33}$$

where $\hat{x}=x/L$, $\hat{t}=t/T_S$, $\hat{\mathbf{A}}_*=T_C\mathbf{A}_*$ (which implies $\hat{\mathbf{E}}_\sigma=T_C\mathbf{E}_\sigma$ and $\hat{\mathbf{E}}_m=T_C\mathbf{E}_m$), and $\hat{\mathbf{V}}=\mathbf{V}/c$. Let us introduce the regular expansion

$$\mathbf{f}_\sigma = \sum_{k=0}^{\infty} \epsilon^k \mathbf{f}_\sigma^{(k)} \tag{34}$$

and then, consequently,

$$\mathbf{m}_\sigma = \sum_{k=0}^{\infty} \epsilon^k \mathbf{m}_\sigma^{(k)}. \tag{35}$$

In particular, for the density and momentum,

$$\rho_\sigma = \sum_{k=0}^{\infty} \epsilon^k \rho_\sigma^{(k)}, \tag{36}$$

$$\hat{\mathbf{j}}_\sigma = \sum_{k=0}^{\infty} \epsilon^k \hat{\mathbf{j}}_\sigma^{(k)}, \tag{37}$$

where $\hat{\mathbf{j}}_\sigma=\rho_\sigma\hat{\mathbf{u}}_\sigma$. Consequently it is possible to define a regular expansion for the velocity—namely,

$$\hat{\mathbf{u}}_\sigma = \frac{\mathbf{j}_\sigma}{\rho_\sigma} = \frac{\sum_{k=0}^{\infty} \epsilon^k \hat{\mathbf{j}}_\sigma^{(k)}}{\sum_{k=0}^{\infty} \epsilon^k \rho_\sigma^{(k)}} = \frac{\hat{\mathbf{j}}_\sigma^{(0)}}{\rho_\sigma^{(0)}} + \epsilon\left(\frac{\hat{\mathbf{j}}_\sigma^{(1)}}{\rho_\sigma^{(0)}} - \frac{\hat{\mathbf{j}}_\sigma^{(0)}}{\rho_\sigma^{(0)}}\frac{\rho_\sigma^{(1)}}{\rho_\sigma^{(0)}}\right) + O(\epsilon^2). \tag{38}$$

In the following, the coefficients of the regular expansion for the momentum $\hat{\mathbf{j}}_\sigma^{(k)}$ will be considered as functions of the coefficients of the regular expansions for the density and velocity—i.e., $\rho_\sigma^{(k)}$ and $\hat{\mathbf{u}}_\sigma^{(k)}$. This means that the expansion given by Eq. (37) means

$$\hat{\mathbf{j}}_\sigma = \rho_\sigma \hat{\mathbf{u}}_\sigma = \left(\sum_{k=0}^{\infty} \epsilon^k \rho_\sigma^{(k)}\right)\left(\sum_{k=0}^{\infty} \epsilon^k \hat{\mathbf{u}}_\sigma^{(k)}\right) = \sum_{k=0}^{\infty} \epsilon^k \left[\sum_{p+q=k} \rho_\sigma^{(p)} \hat{\mathbf{u}}_\sigma^{(q)}\right]. \tag{39}$$

Introducing the previous expansions in the Eq. (33) yields

$$\frac{\partial \mathbf{f}_\sigma^{(k)}}{\partial \hat{t}} + \hat{\mathbf{V}} \cdot \hat{\nabla} \mathbf{f}_\sigma^{(k+1)} = \hat{\mathbf{A}}_* \mathbf{f}_*^{e0}[\rho_\sigma^{(k+2)}] + \hat{\mathbf{A}}_* \sum_{p+q=k+2} \mathbf{f}_*^{e1}[\rho_\sigma^{(p)}, \hat{\mathbf{u}}_\sigma^{(q)}] + \hat{\mathbf{A}}_* \sum_{p+q+r=k+2} \mathbf{f}_*^{e2}[\rho_\sigma^{(p)}, \hat{\mathbf{u}}_\sigma^{(q)}, \hat{\mathbf{u}}_\sigma^{(r)}] - \hat{\mathbf{A}}_* \mathbf{f}_\sigma^{(k+2)}. \tag{40}$$

Conventionally the dependence on the single-species velocity was explicitly reported, even when the barycentric velocity appears in the previous expressions, because the barycentric velocity is the mass average of the species velocity. Since $U/c \ll 1$, then $O(|\mathbf{u}|/c) = \epsilon$ and consequently $\hat{\mathbf{u}}_\sigma^{(0)} = \mathbf{0}$. It has been proved [40] that the expansion coefficients of the moments satisfy the following property:

$$\rho_\sigma^{(2n+1)} = 0, \quad \hat{\mathbf{u}}_\sigma^{(2n)} = \mathbf{0}, \tag{41}$$

for $n \geqslant 0$. Taking into account this property, Eq. (40) for $k=-2$ yields $\mathbf{f}_\sigma^{(0)} = \mathbf{f}_*^{e0}[\rho_\sigma^{(0)}] = \rho_\sigma^{(0)} \mathbf{s}_0$, where $\rho_\sigma^{(0)}$ is unknown. In order to find what macroscopic equation the function $\rho_\sigma^{(0)}$ must satisfy, the equivalent moment formulation with the diffusive scaling will be considered—namely,

$$\epsilon^2 \frac{\partial \mathbf{m}_\sigma}{\partial \hat{t}} + \epsilon \mathbf{M}_A \hat{\mathbf{V}} \cdot (\mathbf{M}_A^{-1} \hat{\nabla} \mathbf{m}_\sigma) = \hat{\mathbf{E}}_* (\mathbf{m}_*^e - \mathbf{m}_\sigma), \tag{42}$$

where $\hat{\mathbf{E}}_* = \hat{\mathbf{E}}_\sigma + \hat{\mathbf{E}}_m$. In particular, introducing the usual expansions in the equations for the lower-order moments and separating the scales yields

$$\frac{\partial \rho_\sigma^{(k)}}{\partial \hat{t}} + \hat{\nabla} \cdot \sum_{p+q=k+1} \rho_\sigma^{(p)} \hat{\mathbf{u}}_\sigma^{(q)} = 0, \tag{43}$$

$$\frac{\partial \hat{\mathbf{j}}_\sigma^{(k)}}{\partial \hat{t}} + \hat{\nabla} \cdot \hat{\mathbf{T}}_\sigma^{(k+1)} = \hat{\lambda}_m^I \sum_{p+q=k+2} \rho_\sigma^{(p)} [\hat{\mathbf{u}}^{(q)} - \hat{\mathbf{u}}_\sigma^{(q)}], \tag{44}$$

where $\hat{\mathbf{T}}_\sigma^{(k+1)} = \hat{\mathbf{V}} \oplus \hat{\mathbf{V}} \oplus \mathbf{f}_\sigma^{(k+1)}$. According to the general property given by Eqs. (41), the Eqs. (43) for $k=-1,+1$ are meaningless. For $k=0,+2$, the same equation yields

$$\frac{\partial \rho_\sigma^{(0)}}{\partial \hat{t}} + \hat{\nabla} \cdot [\rho_\sigma^{(0)} \hat{\mathbf{u}}_\sigma^{(1)}] = 0, \tag{45}$$

$$\frac{\partial \rho_\sigma^{(2)}}{\partial \hat{t}} + \hat{\nabla} \cdot \hat{\mathbf{j}}_\sigma^{(3)} = 0. \tag{46}$$

According to the general property given by Eqs. (41), Eqs. (44) for $k=-2,0$ are meaningless. The equations for $k=-1,+1$ can be recovered:

$$\hat{\nabla} \cdot \hat{\mathbf{T}}_\sigma^{(0)} = \hat{\lambda}_m^I \rho_\sigma^{(0)} [\hat{\mathbf{u}}^{(1)} - \hat{\mathbf{u}}_\sigma^{(1)}], \tag{47}$$

$$\frac{\partial}{\partial \hat{t}} [\rho_\sigma^{(0)} \hat{\mathbf{u}}_\sigma^{(1)}] + \hat{\nabla} \cdot \hat{\mathbf{T}}_\sigma^{(2)} = \hat{\lambda}_m^I [\hat{\mathbf{j}}^{(3)} - \hat{\mathbf{j}}_\sigma^{(3)}]. \tag{48}$$

Recalling the definition of $\mathbf{f}_\sigma^{(0)}$, then $\hat{\mathbf{T}}_\sigma^{(0)} = s_\sigma / 3 \rho_\sigma^{(0)} \mathbf{I}$ and consequently

$$s_\sigma / 3 \hat{\nabla} \rho_\sigma^{(0)} = -\hat{\lambda}_m^I \rho_\sigma^{(0)} \hat{\mathbf{w}}_\sigma^{(1)}, \tag{49}$$

where $\hat{\mathbf{w}}_\sigma^{(1)} = \hat{\mathbf{u}}_\sigma^{(1)} - \hat{\mathbf{u}}^{(1)}$ is the diffusion velocity. Hence in general the leading term of the density field is due to the sum of a constant value ρ_σ^0 and a proper field due to the diffusion velocity $\rho_\sigma^D(\hat{\mathbf{x}})$ satisfying the previous equation—i.e., $\rho_\sigma^{(0)} = \rho_\sigma^0 + \rho_\sigma^D(\hat{\mathbf{x}})$. Equation (40) for $k=-1$ yields

$$\mathbf{f}_\sigma^{(1)} = \mathbf{f}_*^{e1}[\rho_\sigma^{(0)}, \hat{\mathbf{u}}_\sigma^{(1)}] - \hat{\mathbf{A}}_*^\dagger \hat{\mathbf{V}} \cdot \hat{\nabla} \mathbf{f}_\sigma^{(0)}, \tag{50}$$

and recalling the definition of $\mathbf{f}_\sigma^{(0)}$,

$$\mathbf{f}_\sigma^{(1)} = 3 \rho_\sigma^{(0)} \hat{\mathbf{V}} \cdot [\mathbf{s}_I \otimes \hat{\mathbf{u}}^{(1)}] - \hat{\mathbf{A}}_*^\dagger \hat{\mathbf{V}} \cdot [\mathbf{s}_0 \otimes \hat{\nabla} \rho_\sigma^{(0)}]. \tag{51}$$

Applying Eq. (49) yields

$$\mathbf{f}_\sigma^{(1)} = 3 \rho_\sigma^{(0)} \hat{\mathbf{V}} \cdot [\mathbf{s}_I \otimes \hat{\mathbf{u}}^{(1)}] + 3 \rho_\sigma^{(0)} \frac{\hat{\lambda}_m^I}{s_\sigma} \hat{\mathbf{A}}_*^\dagger \hat{\mathbf{V}} \cdot [\mathbf{s}_0 \otimes \hat{\mathbf{w}}_\sigma^{(1)}] \tag{52}$$

and, consequently,

$$\mathbf{f}_\sigma^{(1)} = 3 \rho_\sigma^{(0)} \hat{\mathbf{V}} \cdot [\mathbf{s}_I \otimes \hat{\mathbf{u}}_\sigma^{(1)}]. \tag{53}$$

This result is identical to that obtained by Junk *et al.* [40] for distinct species. Recalling Eq. (40) for $k=0$ and taking into account the general property given by Eq. (41), the last expansion coefficient can be recovered:

$$\mathbf{f}_\sigma^{(2)} = \rho_\sigma^{(2)} \mathbf{s}_I + \mathbf{f}_*^{e2}[\rho_\sigma^{(0)}, \hat{\mathbf{u}}_\sigma^{(1)}, \hat{\mathbf{u}}_\sigma^{(1)}] - \hat{\mathbf{A}}_*^\dagger \left\{ \frac{\partial \mathbf{f}_\sigma^{(0)}}{\partial \hat{t}} + \hat{\mathbf{V}} \cdot [\hat{\nabla} \mathbf{f}_\sigma^{(1)}] \right\}. \tag{54}$$

Assuming $\hat{\lambda}_{\sigma 2}^{II} = \hat{\lambda}_{\sigma 1}^{II}$ and $\hat{\lambda}_{m2}^{II} = \hat{\lambda}_{m1}^{II}$ yields

$$\hat{\mathbf{T}}_\sigma^{(2)} = \left[\frac{s_\sigma}{3} \rho_\sigma^{(2)} + \frac{(2 - s_\sigma)}{3(\hat{\lambda}_{\sigma 3}^{II} + \hat{\lambda}_{m3}^{II})} \frac{\partial \rho_\sigma^{(0)}}{\partial \hat{t}} \right] \mathbf{I} + (1 - \alpha_{\sigma 1}^{II}) \rho_\sigma^{(0)} \mathbf{u}_\sigma^{(1)} \otimes \mathbf{u}_\sigma^{(1)} + \alpha_{\sigma 1}^{II} \rho_\sigma^{(0)} \mathbf{u}^{(1)} \otimes \mathbf{u}^{(1)} - \frac{1}{3(\hat{\lambda}_{\sigma 1}^{II} + \hat{\lambda}_{m1}^{II})} \{ \hat{\nabla} [\rho_\sigma^{(0)} \hat{\mathbf{u}}_\sigma^{(1)}] + \hat{\nabla} [\rho_\sigma^{(0)} \hat{\mathbf{u}}_\sigma^{(1)}]^T - \hat{\nabla} \cdot [\rho_\sigma^{(0)} \hat{\mathbf{u}}_\sigma^{(1)}] \mathbf{I} \} + \beta_{3m1} \rho_\sigma^{(0)} \{ [\hat{\mathbf{u}}^{(1)}]^2 - [\hat{\mathbf{u}}_\sigma^{(1)}]^2 \} \mathbf{I}, \tag{55}$$

where $\beta_{3m1} = (\alpha_{\sigma 3}^{II} - \alpha_{\sigma 1}^{II})/2$. In order to ensure the Galilean invariance of the pressure, $\beta_{3m1} = 0$ is assumed and this implies

$$\frac{\hat{\lambda}_{\sigma 3}^{II}}{\hat{\lambda}_{m3}^{II}} = \frac{\hat{\lambda}_{\sigma 1}^{II}}{\hat{\lambda}_{m1}^{II}}. \tag{56}$$

The asymptotic analysis allows us to define some constraints in the relaxation time constants in order to ensure the desired structure of the macroscopic equations. Taking into account these assumptions, Eq. (48) explicitly becomes

$$\frac{\partial}{\partial \hat{t}}[\rho_\sigma^{(0)}\hat{\mathbf{u}}_\sigma^{(1)}] + \hat{\boldsymbol{\nabla}}\cdot[(1-\alpha_{\sigma 1}^{II})\rho_\sigma^{(0)}\hat{\mathbf{u}}_\sigma^{(1)}\otimes\hat{\mathbf{u}}_\sigma^{(1)} + \alpha_{\sigma 1}^{II}\rho_\sigma^{(0)}\hat{\mathbf{u}}^{(1)} \otimes \hat{\mathbf{u}}^{(1)}] + s_\sigma/3\hat{\boldsymbol{\nabla}}\rho_\sigma^{(2)} = \hat{\boldsymbol{\nabla}}\cdot\{\hat{\nu}_{\sigma m}\hat{\boldsymbol{\nabla}}[\rho_\sigma^{(0)}\hat{\mathbf{u}}_\sigma^{(1)}] + \hat{\nu}_{\sigma m}[\rho_\sigma^{(0)}\hat{\boldsymbol{\nabla}}\hat{\mathbf{u}}_\sigma^{(1)}]^T\} + \hat{\boldsymbol{\nabla}}\{\hat{\eta}_{\sigma m}\hat{\boldsymbol{\nabla}}\cdot[\rho_\sigma^{(0)}\hat{\mathbf{u}}_\sigma^{(1)}]\} + \frac{s_\sigma}{3\hat{D}_\sigma}[\hat{\mathbf{j}}^{(3)} - \hat{\mathbf{j}}_\sigma^{(3)}],, \tag{57}$$

where $\hat{D}_\sigma$, $\hat{\nu}_{\sigma m}$, and $\hat{\eta}_{\sigma m}$ are, respectively, the dimensionless species diffusivity, the kinematic viscosity, and the second coefficient of the kinematic viscosity for the generic species of the mixture, defined as

$$\hat{D}_\sigma = \frac{s_\sigma}{3\hat{\lambda}_m^I}, \tag{58}$$

$$\hat{\nu}_{\sigma m} = \frac{1}{3(\hat{\lambda}_{\sigma 1}^{II} + \hat{\lambda}_{m1}^{II})}, \tag{59}$$

$$\hat{\eta}_{\sigma m} = \frac{2-s_\sigma}{3(\hat{\lambda}_{\sigma 3}^{II} + \hat{\lambda}_{m3}^{II})} - \frac{1}{3(\hat{\lambda}_{\sigma 1}^{II} + \hat{\lambda}_{m1}^{II})}. \tag{60}$$

Collecting the previous results yields

$$\epsilon^2\frac{\partial}{\partial \hat{t}}[\rho_\sigma^{(0)} + \epsilon^2\rho_\sigma^{(2)}] + \epsilon\hat{\boldsymbol{\nabla}}\cdot[\epsilon\rho_\sigma^{(0)}\hat{\mathbf{u}}_\sigma^{(1)} + \epsilon^3\hat{\mathbf{j}}_\sigma^{(3)}] = 0, \tag{61}$$

$$\epsilon^2\frac{\partial}{\partial \hat{t}}[\epsilon\rho_\sigma^{(0)}\hat{\mathbf{u}}_\sigma^{(1)}] + \epsilon\hat{\boldsymbol{\nabla}}\cdot[\epsilon^2(1-\alpha_{\sigma 1}^{II})\rho_\sigma^{(0)}\hat{\mathbf{u}}_\sigma^{(1)}\otimes\hat{\mathbf{u}}_\sigma^{(1)} + \epsilon^2\alpha_{\sigma 1}^{II}\rho_\sigma^{(0)}\hat{\mathbf{u}}^{(1)}\otimes\hat{\mathbf{u}}^{(1)}] + \epsilon s_\sigma/3\hat{\boldsymbol{\nabla}}[\rho_\sigma^{(0)} + \epsilon^2\rho_\sigma^{(2)}] = \epsilon\hat{\boldsymbol{\nabla}}[\hat{\eta}_{\sigma m}\epsilon\hat{\boldsymbol{\nabla}}\cdot(\epsilon\rho_\sigma^{(0)}\hat{\mathbf{u}}_\sigma^{(1)})] + \epsilon\hat{\boldsymbol{\nabla}}\cdot\{\hat{\nu}_{\sigma m}\epsilon\hat{\boldsymbol{\nabla}}[\epsilon\rho_\sigma^{(0)}\hat{\mathbf{u}}_\sigma^{(1)}] + \hat{\nu}_{\sigma m}\epsilon\hat{\boldsymbol{\nabla}}[\epsilon\rho_\sigma^{(0)}\hat{\mathbf{u}}_\sigma^{(1)}]^T\} + \frac{s_\sigma}{3\hat{D}_\sigma}[\rho_\sigma^{(0)}\epsilon\hat{\mathbf{u}}^{(1)} - \rho_\sigma^{(0)}\epsilon\hat{\mathbf{u}}_\sigma^{(1)} + \epsilon^3\hat{\mathbf{j}}^{(3)} - \epsilon^3\hat{\mathbf{j}}_\sigma^{(3)}]. \tag{62}$$

Taking into account that $\hat{t}=t/T_S$, $\hat{\mathbf{x}}=\mathbf{x}/L$, and $\hat{\mathbf{u}}_\sigma^{(1)}=\mathbf{u}_\sigma^{(1)}/c$, it is possible to come back to the original quantities expressed in physical units. Hence, introducing the auxiliary quantities $\tilde{\rho}_\sigma=\rho_\sigma^{(0)}+\epsilon^2\rho_\sigma^{(2)}$ and $\tilde{\mathbf{u}}_\sigma=\epsilon\mathbf{u}_\sigma^{(1)}$, it is easy to verify that they satisfy the following system of equations:

$$\frac{\partial\tilde{\rho}_\sigma}{\partial t} + \boldsymbol{\nabla}\cdot(\tilde{\rho}_\sigma\tilde{\mathbf{u}}_\sigma) = 0, \tag{63}$$

$$\frac{\partial}{\partial t}(\tilde{\rho}_\sigma\tilde{\mathbf{u}}_\sigma) + \boldsymbol{\nabla}\cdot[(1-\alpha_{\sigma 1}^{II})\tilde{\rho}_\sigma\tilde{\mathbf{u}}_\sigma\otimes\tilde{\mathbf{u}}_\sigma + \alpha_{\sigma 1}^{II}\tilde{\rho}_\sigma\tilde{\mathbf{u}}\otimes\tilde{\mathbf{u}}] = -\boldsymbol{\nabla}\tilde{p}_\sigma + \boldsymbol{\nabla}[\eta_{\sigma m}\boldsymbol{\nabla}\cdot(\tilde{\rho}_\sigma\tilde{\mathbf{u}}_\sigma)] + \boldsymbol{\nabla}\cdot[\nu_{\sigma m}\boldsymbol{\nabla}(\tilde{\rho}_\sigma\tilde{\mathbf{u}}_\sigma) + \nu_{\sigma m}\boldsymbol{\nabla}(\tilde{\rho}_\sigma\tilde{\mathbf{u}}_\sigma)^T] - \frac{e_\sigma}{D_\sigma}\tilde{\rho}_\sigma(\tilde{\mathbf{u}}_\sigma - \tilde{\mathbf{u}}) + O(\tilde{\mathbf{u}}_\sigma^3), \tag{64}$$

where $\tilde{p}_\sigma=e_\sigma\tilde{\rho}_\sigma$, $D_\sigma=T_C c^2\hat{D}_\sigma$, $\nu_{\sigma m}=T_C c^2\hat{\nu}_{\sigma m}$, and $\eta_{\sigma m}=T_C c^2\hat{\eta}_{\sigma m}$. Equivalently we can say that $\tilde{\rho}_\sigma$ and $\tilde{\mathbf{u}}_\sigma$, collecting the terms of the numerical solution up to second order with regards to the expansion parameter ϵ, satisfy the Navier-Stokes system of equations with second-order accuracy in space and first-order accuracy in time, because $O(\delta t/\delta x)=\epsilon$.

Obviously summing the governing equations for the single species should yield the mixture equations governing the total density and the barycentric velocity. This implies $\alpha_{\sigma 1}^{II}=1$—i.e., $\hat{\lambda}_{\sigma 1}^{II}=0$—and consequently $\hat{\lambda}_{\sigma 3}^{II}=0$, taking into account Eq. (56). The previous assumptions essentially mean that $\mathbf{f}_*^e=\mathbf{f}_m^e$, coherently with the *single-fluid* approach. This remarkable result was obtained by simply imposing that (a) the pressure must be Galilean invariant and that (b) summing the nonlinear inertial tensor for each species must produce the same term for the mixture. The previous compatibility conditions essentially reduce the Hamel model to the same basic model considered by the *single-fluid* approach. The compatibility conditions remind us that a collision operator involving the local Maxwellian centered on the barycentric velocity—i.e., $\mathbf{f}_m^e$—is the only choice consistent with the continuous kinetic theory [45]. The practical advantage of the proposed model still remains the multiple-relaxation-time formulation, which allows one to tune independently the diffusion coefficient and the viscosity coefficients. For this reason, the claimed main advantage of the *multiple-fluid* approach [28]—i.e., independently tuning the macroscopic transport coefficients—can be easily recovered in the framework of the *single-fluid* approach by considering the MRT formulation.

Finally the last condition required for ensuring the consistent system of equations for the barycentric velocity is that $\nu_{\sigma m}=\nu_m$ and $\eta_{\sigma m}=\eta_m$ for all species. This implies

$$\frac{1}{\lambda_{m3}^{II}} = \frac{3}{2-s_\sigma}\left(\frac{\eta_m}{c^2} + \frac{1}{3\lambda_{m1}^{II}}\right). \tag{65}$$

In this way, the final set of equations for the barycentric quantities can be recovered:

$$\frac{\partial\tilde{\rho}}{\partial t} + \boldsymbol{\nabla}\cdot(\tilde{\rho}\tilde{\mathbf{u}}) = 0, \tag{66}$$

$$\frac{\partial}{\partial t}(\tilde{\rho}\tilde{\mathbf{u}}) + \boldsymbol{\nabla}\cdot(\tilde{\rho}\tilde{\mathbf{u}}\otimes\tilde{\mathbf{u}}) = -\boldsymbol{\nabla}\tilde{p} + \boldsymbol{\nabla}[\eta_m\boldsymbol{\nabla}\cdot(\tilde{\rho}\tilde{\mathbf{u}})] + \boldsymbol{\nabla}\cdot[\nu_m\boldsymbol{\nabla}(\tilde{\rho}\tilde{\mathbf{u}}) + \nu_m\boldsymbol{\nabla}(\tilde{\rho}\tilde{\mathbf{u}})^T], \tag{67}$$

where $\tilde{p}=\Sigma_\sigma\tilde{p}_\sigma$ is the total pressure.

Before proceeding with the numerical integration, as an example, how tuning the transport coefficients for binary mixtures will be discussed.

1. Binary mixtures: Tuning strategy for the mutual diffusivity

Up to now, the diffusion phenomenon was modeled by means of the species diffusivity: in this section, how this concept is related to the mutual diffusivity is outlined. The leading term of Eq. (64) is

$$\tilde{\rho}_\sigma \tilde{\mathbf{w}}_\sigma \approx -D_\sigma \nabla \tilde{\rho}_\sigma, \tag{68}$$

which can be considered as the definition of the species diffusivity D_σ depending on the distinct species molecular weight. Since $D_\sigma = e_\sigma / \lambda_m^I$, then

$$\lambda_m^I (\tilde{\mathbf{u}}_\sigma - \tilde{\mathbf{u}}) \approx -\frac{e_\sigma}{\tilde{\rho}_\sigma} \nabla \tilde{\rho}_\sigma. \tag{69}$$

For explaining how the species diffusivity is related to the mutual diffusivity D, which is the same for all the components of the mixture, let us consider a binary mixture made of particles A and particles B as a meaningful example. Taking the difference between the two expressions derived from the generic equation (69) for species A and B yields

$$\lambda_m^I (\tilde{\mathbf{u}}_A - \tilde{\mathbf{u}}_B) = -\frac{\tilde{p}\tilde{\rho}}{\tilde{\rho}_A \tilde{\rho}_B} \mathbf{d}_{AB}, \tag{70}$$

where M_A and M_B are the molar weights for the two species, M is the molar weight for the mixture, defined as

$$M = \frac{1}{x_A / M_A + x_B / M_B}, \tag{71}$$

and, finally, the driving force is

$$\mathbf{d}_{AB} = \frac{\tilde{\rho}_A \tilde{\rho}_B}{\tilde{p} e \rho} \left[\frac{1}{\tilde{\rho}_A} \nabla (\tilde{\rho}_A e_A) - \frac{1}{\tilde{\rho}_B} \nabla (\tilde{\rho}_B e_B) \right]. \tag{72}$$

Introducing the molar concentrations, defined as $y_A = \tilde{n}_A / \tilde{n}$ and $y_B = \tilde{n}_B / \tilde{n}$ where $\tilde{n}_A$ and $\tilde{n}_B$ are the number densities for the two species, and recalling that for a binary mixture $\nabla y_B = -\nabla y_A$ yields

$$\mathbf{d}_{AB} = \nabla y_A + \frac{\tilde{n}_A \tilde{n}_B}{\tilde{\rho} \tilde{n}} \frac{(M_B - M_A)}{\tilde{n}} \nabla \tilde{n}. \tag{73}$$

We can attribute the discrepancy in the species velocities $(\tilde{\mathbf{u}}_A - \tilde{\mathbf{u}}_B)$ to two different driving mechanisms: the molar concentration gradients and the pressure gradient (which is proportional to the mixture number density for ideal gases) by means of different molar weights ($M_A \neq M_B$). The diffusions driven by these driving mechanisms are called the *ordinary diffusion* and the *pressure diffusion*, respectively.

The mutual diffusivity can be defined by means of the following relation:

$$(\tilde{\mathbf{u}}_A - \tilde{\mathbf{u}}_B) = -\frac{\tilde{n}^2}{\tilde{n}_A \tilde{n}_B} D \mathbf{d}_{AB}. \tag{74}$$

Comparing Eqs. (74) and (70) yields

$$D = \frac{\tilde{p}\tilde{\rho}}{\lambda_m^I \tilde{n}^2 M_A M_B} = \frac{RT / \lambda_m^I}{x_A M_B + x_B M_A}, \tag{75}$$

where R is the universal gas constant and T is the temperature. The previous expression allows one to tune the relaxation frequency λ_m^I in order to recover the experimental data concerning the mutual diffusivity D. A very popular (kinetically derived) formula for the mutual diffusivity [46] is

$$D' = \frac{C'}{\tilde{p} \sigma_{AB}^2 \Omega_D} \sqrt{T^3 \frac{M_A + M_B}{M_A M_B}}, \tag{76}$$

where C' is a proper dimensional constant, σ_{AB} is the characteristic length (arithmetic average of the molecular collision diameters), and finally Ω_D is the collision integral (function of the temperature and the interaction potential). As outlined by means of the asymptotic analysis, the leading term of the total pressure $\tilde{p}^{(0)}$ is essentially constant. This means that, for isothermal conditions, D_k can be approximated as a constant as well. Consequently tuning λ_m^I in such a way to ensure $D = D'$ implies that λ_m^I should depend on the actual mass concentrations. This is not a theoretical problem because the relaxation frequencies involved in the BGK-like collisional operators may depend on any combination of the macroscopic moments (as it happens for the mass concentration). This simply forces us to recalculate the relaxation frequency $\lambda_m^I(x_A)$ for each cell during the calculation, according to the actual value of the local mass concentration, and then to increase substantially the computational demand. However, these additional computations can be avoided if the mass concentration in the computational domain slightly varies around an average value x_A^0, which can be assumed fixed for approximating $\lambda_m^I(x_A^0)$ once for all.

Some final remarks for modeling large particle mass ratios are reported. The distinct species diffusivity D_σ depends on the particle molecular weight, while the mutual diffusivity D is the same for all the mixture components. The tunable parameter s_σ allows one to tune the distinct species diffusivity—i.e., to take into account the effects due to the molecular weight on the diffusion dynamics. Tuning properly this parameter, it is easy to deal with mass particle ratios in the mixture far from unit. Selecting the equilibrium distribution function in such a way that the distinct species diffusivity can be independently adjusted is not a new idea, and it derives from the common practice using the same approach for tuning the actual equation of state (see, for example, [47] for a recent implementation of this idea). In particular the approach proposed in the present paper is much simpler than that discussed in [47] and referred as "same lattice speed" (SLS), because it allows one to model particles with different molecular weights on the same lattice. Unlike the algebraic procedure proposed in the cited paper, the corrective factor s_σ, involved in the effective weight vector given by Eq. (9), has a simple physical interpretation. In fact the ratio between the number of moving particles and the total number of particles in equilibrium conditions can be expressed as

$$\gamma = \frac{5/9 s_\sigma}{(1 - 5/9 s_\sigma) + 5/9 s_\sigma} = \frac{5}{9} s_\sigma, \tag{77}$$

which is simply proportional to s_σ. The common definition of the equilibrium distribution function implies $s_\sigma = 1$ and consequently $\gamma = 5/9$, which means that, in equilibrium conditions, the moving particles are slightly more than the particles at rest. Selecting $s_\sigma \geqslant 1$ is possible to increase the number of moving particles over the total and this can yield to instability. On the other hand, selecting $s_\sigma \leqslant 1$ increases the stability of the calculation by reducing the actual updating

rate during each time step. For dealing with large mass particle ratios, it is enough to select $s_A=1$ if A is the species characterized by the smallest molecular weight and consequently by the fastest dynamics in order to be sure than $s_\sigma \leqslant s_A=1$ for all the other species. Obviously this could increase the computational time for the whole simulation but at least this strategy ensures a stable solution process. Actually the computation time can be effectively reduced by a semi-implicit-linearized formula. Some numerical tests confirming this technique are reported in Sec. V D.

2. Binary mixtures: Tuning strategy for the mixture kinematic viscosity

We can proceed in a very similar way for the mixture viscosities. In the low-Mach-number limit, the essential role is played by the mixture kinematic viscosity, which will be discussed in this section. According to the previously discussed derivation process, in the proposed model the kinematic viscosity is

$$\nu_m = \frac{c^2}{3\lambda_{m1}^{II}}. \tag{78}$$

The previous expression allows one to tune the relaxation frequency λ_{m1}^{II} in order to recover the experimental data concerning the mixture kinematic viscosity ν_m. A very popular (experimental) formula for the mixture kinematic viscosity is [46]

$$\nu_m' = \frac{x_A \nu_A}{1 + F_{AB}(M_A/M_B)(x_B/x_A)} + \frac{x_B \nu_B}{1 + F_{BA}(M_B/M_A)(x_A/x_B)}, \tag{79}$$

where F_{AB} and F_{BA} are positive corrective factors. In particular the experimental data show that the effective kinematic viscosity for the mixture is smaller than the averaged viscosity based on the mass concentrations of the components $\nu_m' \leqslant \Sigma_\sigma x_\sigma \nu_\sigma$. This means that the actual mixture kinematic viscosity is a function of the mass concentration x_A—namely, $\nu_m'(x_A)$. In particular the fact that $\nu_m'(0)=\nu_B$ and $\nu_m'(1)=\nu_A$ ensures the required consistency with the single-species case, because the mixture kinematic viscosity reduces to the disting species viscosity of the residual component. Since for binary mixtures also the barycentric velocity $\tilde{\mathbf{u}}(x_A)$—reduces to the actual velocity of the residual component—i.e., $\tilde{\mathbf{u}}(0)=\tilde{\mathbf{u}}_B$ and $\tilde{\mathbf{u}}(1)=\tilde{\mathbf{u}}_A$—then the single-species momentum equation is correctly recovered. Again tuning λ_{m1}^{II} in such a way to ensure $\nu_m=\nu_m'$ implies that λ_{m1}^{II} should depend on the actual mass concentration. Even though the same considerations discussed in the previous section hold, neglecting the dependence on the mass concentration in this case will not allow us to be consistent any more with the single-species case, at least as far as the correct transport coefficients in the momentum equation are concerned.

In the next section, some integration formulas will be compared in order to analyze the performance of the numerical implementations of the previous model.

IV. NUMERICAL IMPLEMENTATION

A. Semi-implicit formulation

Let us introduce the one-dimensional array $\vec{\mathbf{f}}_\sigma(\hat{t},\hat{\mathbf{X}}) = \{f_\sigma^i[\hat{t},\hat{\mathbf{X}}^T\hat{\mathbf{e}}(i)]\}$, where $\mathbf{f}_\sigma(\hat{t},\hat{\mathbf{x}})$ is the usual distribution vector at the generic time $\hat{t}$ and for the generic point $\hat{\mathbf{x}}$ and $\hat{\mathbf{e}}(i) \in \mathbb{R}^9$ is the unit vector for the ith generic lattice velocity. For definition, it is easy to verify that $\vec{\mathbf{f}}_\sigma(\hat{t},1\otimes\hat{\mathbf{x}})=\mathbf{f}_\sigma(\hat{t},\hat{\mathbf{x}})$. The arrow notation was selected for pointing out that the vector $\vec{\mathbf{f}}_\sigma$ collects the components of the discrete distribution functions of neighboring cells, according to the considered direction of the lattice.

Equation (27) can be expressed as

$$\frac{D}{D\hat{t}_c}\vec{\mathbf{f}}_\sigma(\hat{t}_c,\hat{\mathbf{X}}_c) = \hat{\mathbf{A}}_*[\vec{\mathbf{f}}_*^e(\hat{t}_c,\hat{\mathbf{X}}_c) - \vec{\mathbf{f}}_\sigma(\hat{t}_c,\hat{\mathbf{X}}_c)], \tag{80}$$

where $\hat{\mathbf{X}}_c=1\otimes\hat{\mathbf{x}}_c$, $\hat{\mathbf{x}}_c$ is the generic location divided by the spatial discretization step $\hat{\mathbf{x}}_c=\mathbf{x}/\delta x$, and $\hat{t}_c$ is the generic time divided by the time step $\hat{t}_c=t/\delta t$.

Since a fixed set of lattice velocities is considered, the theory of characteristics is highly simplified for the lattice Boltzmann method and hence it becomes particularly advantageous for the discretization. However, it is well known that this is not mandatory [48]. In fact a Eulerian interpretation of the previous equations allows one to independently discretize the spatial and time derivatives. This is particularly advantageous for enhancing the accuracy of the spatial discretization without increasing the number of time steps. The Eulerian formulation will be presented first, while the conventional Lagrangian formulation will be presented in the next sections.

Let us store all the components of $\mathbf{f}_\sigma(\hat{t}_c,\hat{\mathbf{x}}_c)$ of all grid nodes $\hat{\mathbf{x}}_c$ in a one-dimensional array $\bar{\mathbf{f}}_\sigma(\hat{t}_c)$ using an appropriate ordering. The overbar notation was selected for pointing out that all the computational cells are considered in the one-dimensional vector $\bar{\mathbf{f}}_\sigma$, which is actually much larger than the single-cell vector $\mathbf{f}_\sigma$ because of the mesh size. Applying a proper spatial discretization formula yields

$$\frac{d}{d\hat{t}_c}\bar{\mathbf{f}}_\sigma(\hat{t}_c) + \bar{\mathbf{M}}_A\bar{\mathbf{f}}_\sigma(\hat{t}_c) = \bar{\mathbf{A}}_*[\bar{\mathbf{f}}_*^e(\hat{t}_c) - \bar{\mathbf{f}}_\sigma(\hat{t}_c)], \tag{81}$$

where $\bar{\mathbf{A}}_*=\mathrm{blkdiag}(\hat{\mathbf{A}}_*)$ is the block-diagonal matrix obtained by the concatenation of the matrix $\hat{\mathbf{A}}_*$ and $\bar{\mathbf{M}}_A$ is the advection operator due to the considered spatial discretization formula. The equilibrium distribution vector can be split, taking into account the order of the involved terms with regards to the macroscopic velocity. Moreover, the terms which do not depend or linearly depend on the velocity can be expressed by means of the operators $\mathbf{M}_{e0}$ and $\mathbf{M}_{e1}$—namely,

$$\mathbf{f}_*^{e0}(\hat{t}_c,\hat{\mathbf{x}}_c) = \mathbf{M}_{e0}\mathbf{f}_\sigma(\hat{t}_c,\hat{\mathbf{x}}_c), \tag{82}$$

$$\mathbf{f}_\sigma^{e1}(\hat{t}_c,\hat{\mathbf{x}}_c) = \mathbf{M}_A^{-1}\rho_\sigma[0,u_{\sigma x},u_{\sigma y},0,0,0,0,0,0]^T = \mathbf{M}_{e1}\mathbf{f}_\sigma(\hat{t}_c,\hat{\mathbf{x}}_c), \tag{83}$$

$$\mathbf{f}_{mm}^{e1}(\hat{t}_c,\hat{\mathbf{x}}_c)=\mathbf{M}_A^{-1}\rho[0,u_x,u_y,0,0,0,0,0,0]^T=\mathbf{M}_{e1}\sum_{\tau}\mathbf{f}_{\tau}(\hat{t}_c,\hat{\mathbf{x}}_c), \tag{84}$$

$$\mathbf{f}_{*}^{e1}(\hat{t}_c,\hat{\mathbf{x}}_c)=\mathbf{M}_A^{-1}\rho_{\sigma}[0,u_x,u_y,0,0,0,0,0,0]^T = x_{\sigma}(\hat{t}_c,\hat{\mathbf{x}}_c)\mathbf{M}_{e1}\sum_{\tau}\mathbf{f}_{\tau}(\hat{t}_c,\hat{\mathbf{x}}_c), \tag{85}$$

where $x_\sigma=\rho_\sigma/\rho$ is the mass concentration. Introducing the previous operators in Eq. (81) yields

$$\frac{d}{d\hat{t}_c}\bar{\mathbf{f}}_{\sigma}(\hat{t}_c)=(\bar{\mathbf{A}}_*\bar{\mathbf{M}}_{e0}-\bar{\mathbf{M}}_A-\bar{\mathbf{A}}_*)\bar{\mathbf{f}}_{\sigma}(\hat{t}_c)+\bar{\mathbf{A}}_*\bar{\mathbf{M}}_{e1}^{\sigma}\sum_{\tau}\bar{\mathbf{f}}_{\tau}(\hat{t}_c)+\bar{\mathbf{A}}_*\bar{\mathbf{f}}_{*}^{e2}(\hat{t}_c), \tag{86}$$

where $\bar{\mathbf{M}}_{e0}=\mathrm{blkdiag}(\mathbf{M}_{e0})$ and $\bar{\mathbf{M}}_{e1}^{\sigma}=\mathrm{blkdiag}(x_\sigma\mathbf{M}_{e1})$. Applying a proper multistep time discretization formula yields

$$\begin{aligned}\sum_{n=0}^{N_s}\bar{\mathbf{M}}_n\bar{\mathbf{f}}_{\sigma}(\hat{t}_c-n)=&-\bar{\mathbf{M}}_A[\theta_A\bar{\mathbf{f}}_{\sigma}(\hat{t}_c)+(1-\theta_A)\bar{\mathbf{f}}_{\sigma}(\hat{t}_c-1)]\\&+\bar{\mathbf{A}}_*(\bar{\mathbf{M}}_{e0}-\bar{\mathbf{I}})[\theta_0\bar{\mathbf{f}}_{\sigma}(\hat{t}_c)+(1-\theta_0)\bar{\mathbf{f}}_{\sigma}(\hat{t}_c-1)]\\&+\bar{\mathbf{A}}_*[\theta_1\bar{\mathbf{M}}_{e1}^{\sigma}(\hat{t}_c)+(1-\theta_1)\bar{\mathbf{M}}_{e1}^{\sigma}(\hat{t}_c-1)]\\&\times\sum_{\tau}[\theta_1\bar{\mathbf{f}}_{\tau}(\hat{t}_c)+(1-\theta_1)\bar{\mathbf{f}}_{\tau}(\hat{t}_c-1)]\\&+\bar{\mathbf{A}}_*[\theta_2\bar{\mathbf{f}}_{*}^{e2}(\hat{t}_c)+(1-\theta_2)\bar{\mathbf{f}}_{*}^{e2}(\hat{t}_c-1)],\end{aligned} \tag{87}$$

where N_s is the number of time steps and $\bar{\mathbf{M}}_n$ are the matrices due the considered time integration formula. Even though the previous formulation is not the most general, it allows one to discuss some approaches proposed in literature.

(i) If one assumes $\theta_A=\theta_0=\theta_1=\theta_2=0$, then the conventional fully explicit approach (E) is recovered. In this case, the integration process is explicitly time marching and only the results due to the previous iterations are needed in order to compute the next time step. This approach is very simple to implement but requires that the relaxation frequencies be smaller than a given stability threshold and this could dramatically increase the computational time—for example, dealing with reactive mixtures characterized by very small reaction rates.

(ii) The simple remedy to the previous problem is obviously the fully implicit approach (I), which means $\theta_A=\theta_0=\theta_1=\theta_2=1$. The idea for the lattice Boltzmann method was proposed some time ago [10,49,50], and it enjoyed some moderate success in applications [51–55]. The stability threshold for the relaxation frequencies completely disappears, but the additional computations required by solving a global nonlinear set of equations can sometimes reduce the practical advantage. For simulating a given time frame of the physical problem, one needs fewer time steps but each one of them is longer to be computed. In particular, it has been shown that the practical advantage due to the implicit formulation in avoiding any stability threshold can be sometimes overcome by the increased computational demand [56,57].

(iii) Some approaches in between were proposed too. The main drawbacks of the fully implicit approach is that it must deal with a global nonlinear set of equations. The set of equations is global because of the advection term—i.e., $\bar{\mathbf{M}}_A$. Some papers [58,59] proposed a semi-implicit nonlinear approach (SINL), which means $\theta_A=0$ and $\theta_0=\theta_1=\theta_2=1$, with the advantage that the nonlinear system to be solved is local and hence much smaller, since the advection part is solved explicitly. However, during the computation of each cell a small nonlinear set of equations must be solved and the final effect on the computational demand can be still relevant.

(iv) Actually according to the asymptotic analysis discussed in the previous section, the quadratic term involved in the generalized equilibrium distribution function—i.e., $\mathbf{f}_*^{e2}$—does not affect too much the macroscopic equations. In particular, this term will determine the second-order expansion coefficient $\mathbf{f}_\sigma^{(2)}$ and consequently the nonlinear inertial term in the macroscopic momentum equation. It is easy to verify that an error $O(\epsilon)$ in dealing with $\mathbf{f}_*^{e2}$ does not produce any effect on the macroscopic equations if terms $O(\epsilon^3)$ are neglected (consistently with the discussed accuracy goals). For this reason in this paper, we propose a SIL approach, which means $\theta_A=\theta_2=0$ and $\theta_0=\theta_1=1$. In this way, the most important terms in the collision operator effecting the stability are still solved implicitly but the operative matrices can be derived once for all at the beginning of the calculation by means of simple algebra.

B. Memory-optimized (single-step) integration formulas

As previously discussed referring to the Eulerian interpretation of the lattice Boltzmann method, the practical advantage of independently discretizing the spatial and time derivatives holds for $N_s=1$—i.e., single-step integration formulas—because in this case only the results due to the previous iteration must be stored in memory.

Let us store all the components of $\vec{\mathbf{f}}_\sigma(\hat{t}_c,1\otimes\hat{\mathbf{x}}_c-\hat{\mathbf{V}}_c)$ of all grid nodes $\hat{\mathbf{x}}_c$ in a one-dimensional array $\bar{\mathbf{f}}_\sigma^{up}(\hat{t}_c)$. Let us introduce the up-wind operator—namely,

$$\bar{\mathbf{f}}_{\sigma}^{up}(\hat{t}_c)=\bar{\mathbf{M}}_{up}\bar{\mathbf{f}}_{\sigma}(\hat{t}_c). \tag{88}$$

In the same way, it is possible to introduce the down-wind operator—namely,

$$\bar{\mathbf{f}}_{\sigma}^{dw}(\hat{t}_c)=\bar{\mathbf{M}}_{dw}\bar{\mathbf{f}}_{\sigma}(\hat{t}_c), \tag{89}$$

where $\bar{\mathbf{f}}_\sigma^{dw}(\hat{t}_c)$ is the one-dimensional array storing all the components of $\vec{\mathbf{f}}_\sigma(\hat{t}_c,\mathbf{1}\otimes\hat{\mathbf{x}}_c+\hat{\mathbf{V}}_c)$. A possible choice for the advection matrix ensuring third-order accuracy is

$$\bar{\mathbf{M}}_A=\frac{1}{3}\bar{\mathbf{M}}_{dw}+\frac{1}{2}\bar{\mathbf{I}}-\bar{\mathbf{M}}_{up}+\frac{1}{6}\bar{\mathbf{M}}_{up}^2. \tag{90}$$

1. General diffusion phenomena

Approximating the time derivative by means of the Euler formula—i.e., $\bar{\mathbf{M}}_0=-\bar{\mathbf{M}}_1=\bar{\mathbf{I}}$—and assuming the

semi-implicit-linearized formulation—i.e., $\theta_A=\theta_2=0$ and $\theta_0=\theta_1=1$—yields

$$\bar{\mathbf{f}}_\sigma(\hat{t}_c)-\bar{\mathbf{A}}_*(\bar{\mathbf{M}}_{e0}-\bar{\mathbf{I}})\bar{\mathbf{f}}_\sigma(\hat{t}_c)-\bar{\mathbf{A}}_*\bar{\mathbf{M}}^\sigma_{e1}(\hat{t}_c)\sum_\tau\bar{\mathbf{f}}_\tau(\hat{t}_c)$$

$$=(\bar{\mathbf{I}}-\bar{\mathbf{M}}_A)\bar{\mathbf{f}}_\sigma(\hat{t}_c-1)+\bar{\mathbf{A}}_*\bar{\mathbf{f}}^{e2}_*(\hat{t}_c-1). \quad (91)$$

Summing over all the species it is possible to derive the operative formula for updating the mixture distribution function during each time step—namely,

$$\sum_\tau\bar{\mathbf{f}}_\tau(\hat{t}_c)=[\bar{\mathbf{I}}-\bar{\mathbf{A}}_*(\bar{\mathbf{M}}_{e0}-\bar{\mathbf{I}})-\bar{\mathbf{A}}_*\bar{\mathbf{M}}_{e1}(\hat{t}_c)]^{-1}$$

$$\left[(\bar{\mathbf{I}}-\bar{\mathbf{M}}_A)\sum_\tau\bar{\mathbf{f}}_\tau(\hat{t}_c-1)+\bar{\mathbf{A}}_*\sum_\tau\bar{\mathbf{f}}^{e2}_*(\hat{t}_c-1)\right], \quad (92)$$

where $\bar{\mathbf{M}}_{e1}=\mathrm{blkdiag}(\mathbf{M}_{e1})$. Once the mixture distribution function was computed, the final operative formula for the distinct species distribution function is

$$\bar{\mathbf{f}}_\sigma(\hat{t}_c)=[\bar{\mathbf{I}}-\bar{\mathbf{A}}_*(\bar{\mathbf{M}}_{e0}-\bar{\mathbf{I}})]^{-1}$$

$$\left[(\bar{\mathbf{I}}-\bar{\mathbf{M}}_A)\bar{\mathbf{f}}_\sigma(\hat{t}_c-1)+\bar{\mathbf{A}}_*\bar{\mathbf{M}}^\sigma_{e1}(\hat{t}_c)\sum_\tau\bar{\mathbf{f}}_\tau(\hat{t}_c)+\bar{\mathbf{A}}_*\bar{\mathbf{f}}^{e2}_*(\hat{t}_c-1)\right], \quad (93)$$

where $\Sigma_\tau\bar{\mathbf{f}}_\tau(\hat{t}_c)$ is computed by means of Eq. (92). The previous scheme will be referred in the following as SBDF3, meaning a simplified version of the backward differentiation formula (BDF) with third order, which will be discussed in the next section. In fact, as the third-order BDF, the present formula involves the values of the distribution function in four spatial locations, but at the same time (and this is the advantageous difference). Actually the name would be not completely appropriate because the advection discretization given by matrix $\bar{\mathbf{M}}_A$ is not completely "backward," since also a down stream location was considered for stability reasons.

2. Simple diffusion phenomena

If the total pressure gradient acting on the mixture is small and there is no external force, the barycentric velocity is very small and it can be neglected. In this case, the set of equations (86) can be simplified—namely,

$$\frac{d}{d\hat{t}_c}\bar{\mathbf{f}}_\sigma(\hat{t}_c)=\bar{\mathbf{R}}\bar{\mathbf{f}}_\sigma(\hat{t}_c), \quad (94)$$

where $\bar{\mathbf{R}}=\bar{\mathbf{A}}_*\bar{\mathbf{M}}_{e0}-\bar{\mathbf{M}}_A-\bar{\mathbf{A}}_*$. In this case, any Runge-Kutta methods can be fruitfully applied. In the following sections, the implicit Runge-Kutta-Gauss method with forth order accuracy will be considered (RKG4).

C. Speed-optimized (multiple-step) integration formulas

In order to reduce the computational demand, the theory of characteristics, which is simplified in the framework of the lattice Boltzmann Method, will be considered again, because it allows one to discretize the inertial and advection terms at the same time.

Let us introduce the operator $\vec{\mathbf{F}}_\sigma(\hat{t},\hat{\mathbf{X}})=\{f^j_\sigma[\hat{t},\hat{\mathbf{X}}^T\hat{\mathbf{e}}(i)]\}$ for the actual values of the distribution functions and $\vec{\mathbf{F}}^e_*(\hat{t},\hat{\mathbf{X}})=\{f^{ej}_*[\hat{t},\hat{\mathbf{X}}^T\hat{\mathbf{e}}(i)]\}$ for the equilibrium values of the distribution functions. For definition, it is easy to verify that $\vec{\mathbf{F}}_\sigma(\hat{t},\mathbf{1}\otimes\hat{\mathbf{x}})=\mathbf{1}\otimes\mathbf{f}_\sigma(\hat{t},\hat{\mathbf{x}})$ and a similar expression holds for the equilibrium operator.

Moving along the characteristics defined by the lattice velocities, the set of equations (80) can be immediately considered as a set of ordinary differential equations. This set can be discretized by any multistep formula—namely,

$$\sum_{n=0}^{N_s}\beta_n\vec{\mathbf{f}}_\sigma(\hat{t}_c-n,\hat{\mathbf{X}}_c-n\hat{\mathbf{V}})$$

$$=-\hat{\mathbf{A}}_*\cdot\left\{\theta_0\vec{\mathbf{F}}_\sigma(\hat{t}_c,\hat{\mathbf{X}}_c)+(1-\theta_0)\vec{\mathbf{F}}_\sigma(\hat{t}_c-1,\hat{\mathbf{X}}_c-\hat{\mathbf{V}})\right.$$

$$\left.-\sum_{k=0}^{2}[\theta_k\vec{\mathbf{F}}^{ek}_*(\hat{t}_c,\hat{\mathbf{X}}_c)+(1-\theta_k)\vec{\mathbf{F}}^{ek}_*(\hat{t}_c-1,\hat{\mathbf{X}}_c-\hat{\mathbf{V}})]\right\}. \quad (95)$$

Even though the previous formulation is not completely general, it allows one to recover the following schemes: (i) forward Euler (FE), which means $N_s=1$, $\beta_0=1$, $\beta_1=-1$, and $\theta_0=\theta_1=\theta_2=0$; (ii) backward Euler (BE), which means $N_s=1$, $\beta_0=1$, $\beta_1=-1$, $\theta_0=\theta_1=1$, and $\theta_2=0$; (iii) backward differentiation formula with second-order accuracy (BDF2), which means $N_s=2$, $\beta_0=3/2$, $\beta_1=-2$, $\beta_2=1/2$, $\theta_0=\theta_1=1$, and $\theta_2=0$; (iv) backward differentiation formula with third-order accuracy (BDF3), which means $N_s=3$, $\beta_0=11/6$, $\beta_1=-3$, $\beta_2=3/2$, $\beta_3=-1/3$, $\theta_0=\theta_1=1$, and $\theta_2=0$.

D. Semi-implicit-linearized backward-Euler formula

None of the previously discussed scheme is completely suitable for dealing with mixture modeling in very large applications. The ideal scheme for solving the lattice Boltzmann equation should be (i) *consistent* at least up to the *second* or *third* order in space, for correctly solving the Navier-Stokes equations up to the second order in space for the mixture alone or the mixture together with each distinct species, respectively (see the asymptotic analysis for the discrete model in the next section: in order to recover correctly the momentum equation for each distinct species, an additional accuracy is required because $\rho^{(0)}_\sigma$ is no more constant); (ii) *stable* for a large range of dimensionless relaxation frequencies ($\hat{\lambda}$), allowing one to consider large time step and/or large discrepancies in the macroscopic transport coefficients (this condition is essentially satisfied by *implicit* and *semi-implicit* schemes); (iii) *local*—namely, requiring a very small amount of information from the neighboring cells in order to reduce the communication demand in parallel implementations (roughly speaking the communication demand linearly increases with the number of neighboring locations required by the scheme).

Without entering too much in details, the scheme FE is local but not widely stable neither accurate (if we neglect for a while the usual practice of incorporating the discretization error in the transport coefficients). The scheme BE is local and widely stable, but it is characterized by the same moderate accuracy of the previous one. Finally, the schemes RKG4, BDF2, and BDF3 are not local but they ensure wide stability and good accuracy.

Actually SBDF3 seems a promising idea for recovering the desired accuracy because it introduces some errors in the estimation of the time derivatives only, which are characterized by a slow dynamics $O(\epsilon^2)$, as far as the diffusive scaling is concerned. Unfortunately SBDF3 is not local or widely stable, as will be outlined by means of numerical simulations.

In the following, a scheme is proposed called the semi-implicit-linearized backward-Euler formula, which is essentially a semi-implicit formulation of the backward Euler formula with some proper corrections in order to increase the accuracy. According to this technique, the operative formula is

$$\begin{aligned}\mathbf{f}_\sigma(\hat{t}_c,\hat{\mathbf{x}}_c)-\vec{\mathbf{f}}_\sigma(\hat{t}_c-1,\hat{\mathbf{X}}_c-\hat{\mathbf{V}})=\hat{\mathbf{A}}_*[&\mathbf{f}_*^{e0}(\hat{t}_c,\hat{\mathbf{x}}_c)+\mathbf{f}_*^{e1}(\hat{t}_c,\hat{\mathbf{x}}_c)\\&+\mathbf{f}_*^{e2}(\hat{t}_c-1,\hat{\mathbf{x}}_c)-\mathbf{f}_\sigma(\hat{t}_c,\hat{\mathbf{x}}_c)\\&+\mathbf{k}(\hat{t}_c,\hat{\mathbf{x}}_c)],\end{aligned}\tag{96}$$

where

$$\mathbf{k}(\hat{t}_c,\hat{\mathbf{x}}_c)=\rho_\sigma\mathbf{M}_A^{-1}[0,\hat{b}_x,\hat{b}_y,0,0,0,0,0,0]^T\tag{97}$$

and $\hat{\mathbf{b}}$ is a forcing term which is proportional to the actual value of the diffusion velocity—namely, $\hat{\mathbf{b}}=-m\rho_\sigma\hat{\mathbf{w}}_\sigma$ with m as a freely tunable parameter (*first correction*). This means that the first-order terms with regards to the macroscopic velocities can be grouped together—namely,

$$\begin{aligned}\mathbf{f}_*^{e1}(\hat{t}_c,\hat{\mathbf{x}}_c)+\mathbf{k}(\hat{t}_c,\hat{\mathbf{x}}_c)&=\rho_\sigma\mathbf{M}_A^{-1}[0,(1+m)\hat{u}_x-m\hat{u}_{\sigma x},\hat{u}_y\\&\quad-m\hat{u}_{\sigma y},0,0,0,0,0,0]^T\\&=(1+m)x_\sigma(\hat{t}_c,\hat{\mathbf{x}}_c)\mathbf{f}_{mm}^{e1}(\hat{t}_c,\hat{\mathbf{x}}_c)\\&\quad-m\mathbf{f}_\sigma^{e1}(\hat{t}_c,\hat{\mathbf{x}}_c),\end{aligned}\tag{98}$$

where $\mathbf{f}_{mm}^{e1}(\hat{t}_c,\hat{\mathbf{x}}_c)=\mathbf{M}_{e1}\Sigma_\tau\mathbf{f}_\tau(\hat{t}_c,\hat{\mathbf{x}}_c)$. Coherently with the semi-implicit-linearized approach, the actual mass concentration $x_\sigma(\hat{t}_c,\hat{\mathbf{x}}_c)$ could represent a problem because it involves the single-species density at the new time step. This means that in the updating equation (time marching equation) for the single species, a macroscopic moment of the same species appears at the new time step, which is still unknown. Fortunately the collision step preserves the total number of particles (due to the continuity constraint) and the new species density can be easily computed by means of the post-streaming values of the discrete distribution function. The previous expression can be written as

$$\begin{aligned}&\mathbf{f}_*^{e1}(\hat{t}_c,\hat{\mathbf{x}}_c)+\mathbf{k}(\hat{t}_c,\hat{\mathbf{x}}_c)\\&\quad=\mathbf{M}_{e1}\left[(1+m)x_\sigma(\hat{t}_c,\hat{\mathbf{x}}_c)\sum_\tau\mathbf{f}_\tau(\hat{t}_c,\hat{\mathbf{x}}_c)-m\mathbf{f}_\sigma(\hat{t}_c,\hat{\mathbf{x}}_c)\right].\end{aligned}\tag{99}$$

Introducing the previous expressions into Eq. (96) and summing over the species yields

$$\sum_\tau\mathbf{f}_\tau(\hat{t}_c,\hat{\mathbf{x}}_c)=\mathbf{B}_S\sum_\tau\vec{\mathbf{f}}_\tau(\hat{t}_c-1,\hat{\mathbf{X}}_c-\hat{\mathbf{V}})+\mathbf{B}_Q\sum_\tau\mathbf{f}_*^{e2}(\hat{t}_c-1,\hat{\mathbf{x}}_c),\tag{100}$$

where

$$\mathbf{B}_S=[\mathbf{I}-\hat{\mathbf{A}}_*(\mathbf{M}_{e0}-\mathbf{I})-\hat{\mathbf{A}}_*\mathbf{M}_{e1}]^{-1}\tag{101}$$

and $\mathbf{B}_Q=\mathbf{B}_S\hat{\mathbf{A}}_*$. Equation (100) is the operative time marching formula for updating the mixture distribution function: it is worth the effort to point out that, on the right-hand side of this equation, only the information of the neighboring cells at the previous time step is needed. Once the term $\Sigma_\tau\mathbf{f}_\tau(\hat{t}_c,\hat{\mathbf{x}}_c)$ is known, then it is possible to compute the species dynamics—namely,

$$\begin{aligned}\mathbf{f}_\sigma(\hat{t}_c,\hat{\mathbf{x}}_c)=\mathbf{S}_S\vec{\mathbf{f}}_\sigma(\hat{t}_c-1,\hat{\mathbf{X}}_c-\hat{\mathbf{V}})+\mathbf{S}_Q\mathbf{f}_*^{e2}(\hat{t}_c-1,\hat{\mathbf{x}}_c)\\+x_\sigma(\hat{t}_c,\hat{\mathbf{x}}_c)\mathbf{S}_C\sum_\tau\mathbf{f}_\tau(\hat{t}_c,\hat{\mathbf{x}}_c),\end{aligned}\tag{102}$$

where

$$\mathbf{S}_S=[\mathbf{I}-\hat{\mathbf{A}}_*(\mathbf{M}_{e0}-\mathbf{I})+m\hat{\mathbf{A}}_*\mathbf{M}_{e1}]^{-1},\tag{103}$$

$\mathbf{S}_Q=\mathbf{S}_S\hat{\mathbf{A}}_*$, and $\mathbf{S}_C=(1+m)\mathbf{S}_S\hat{\mathbf{A}}_*\mathbf{M}_{e1}$. Also, for the distinct species dynamics, the operative time marching formula only depends on the information of the neighboring cells at the previous time step. The matrix $\mathbf{S}_C$ represents the coupling due to cross collisions governing the diffusion process. Moreover, the matrices $\mathbf{B}_S$, $\mathbf{B}_Q$, $\mathbf{S}_S$, $\mathbf{S}_Q$, and $\mathbf{S}_C$ are small matrices ($\in\mathbb{R}^{9\times9}$) which depend only on the dimensionless relaxation frequencies ($\hat{\lambda}$): hence they can be computed once for all at the beginning of the calculation, being the same for all the cells.

In the next section, the suitability of the SILBE scheme for solving the Navier-Stokes equations for mixture modeling will be proved by means of the asymptotic analysis.

E. Asymptotic analysis of the MRT Hamel model integrated by the SILBE formula

Let us analyze the SILBE scheme by means of the asymptotic analysis. Applying the Taylor expansion yields

$$\vec{\mathbf{f}}_\sigma(\hat{t}_c-1,\hat{\mathbf{X}}_c-\hat{\mathbf{V}})=\mathbf{f}_\sigma(\hat{t}_c,\hat{\mathbf{x}}_c)+\sum_{k=1}^{\infty}(-\partial/\partial\hat{t}_c-\hat{\mathbf{V}}\cdot\hat{\boldsymbol{\nabla}}_c)^k\mathbf{f}_\sigma(\hat{t}_c,\hat{\mathbf{x}}_c),\tag{104}$$

$$\mathbf{f}_*^{e2}(\hat{t}_c-1,\hat{\mathbf{x}}_c)=\mathbf{f}_*^{e2}(\hat{t}_c,\hat{\mathbf{x}}_c)+\sum_{k=1}^{\infty}(-\partial/\partial\hat{t}_c)^k\mathbf{f}_*^{e2}(\hat{t}_c,\hat{\mathbf{x}}_c). \tag{105}$$

It is worth the effort of recalling that both time $\hat{t}_c$ and space $\hat{\mathbf{x}}_c$ are the dimensionless quantities used in the code. However, this dimensionless coordinates are not representative of the physical dynamics described by the diffusive scaling or, equivalently, if the diffusive scaling holds, then $O(\hat{t}_c)\neq 1$ and $O(\hat{\mathbf{x}}_c)\neq 1$. For this reason, recalling that $\hat{t}_c=\hat{t}/\epsilon^2$ and $\hat{\mathbf{X}}_c=\hat{\mathbf{X}}/\epsilon$, it is possible to rewrite the previous Taylor expansions as

$$\vec{\mathbf{f}}_\sigma(\hat{t}/\epsilon^2-1,\hat{\mathbf{X}}/\epsilon-\hat{\mathbf{V}})=\mathbf{f}_\sigma(\hat{t}/\epsilon^2,\hat{\mathbf{x}}/\epsilon)+\sum_{k=1}^{\infty}(-\epsilon^2\partial/\partial\hat{t}-\epsilon\hat{\mathbf{V}}\cdot\hat{\nabla})^k\mathbf{f}_\sigma(\hat{t}/\epsilon^2,\hat{\mathbf{x}}/\epsilon), \tag{106}$$

$$\mathbf{f}_*^{e2}(\hat{t}/\epsilon^2-1,\hat{\mathbf{x}}/\epsilon)=\sum_{k=0}^{\infty}\epsilon^{2k}(-\partial/\partial\hat{t})^k\mathbf{f}_*^{e2}(\hat{t}/\epsilon^2,\hat{\mathbf{x}}/\epsilon). \tag{107}$$

First of all, introducing the previous expansions in Eq. (96) allows one to express the finite-difference operative formula by means of differential operators—namely,

$$-\sum_{k=1}^{\infty}[\epsilon^k D_k(-\partial/\partial\hat{t},-\hat{\mathbf{V}}\cdot\hat{\nabla})\mathbf{f}_\sigma+\epsilon^{2k}\hat{\mathbf{A}}_*(-\partial/\partial\hat{t})^k\mathbf{f}_*^{e2}]=\hat{\mathbf{A}}_*(\mathbf{f}_*^e-\mathbf{f}_\sigma+\mathbf{k}), \tag{108}$$

where $D_k(x_1,x_2)$ are polynomials defined as $D_0(x_1,x_2)=0$ and

$$D_k(x_1,x_2)=\sum_{2a+b=k\geqslant 1}\frac{x_1^a x_2^b}{a!b!}. \tag{109}$$

Separating the scales yields

$$-\sum_{p+q=k+2}D_p(-\partial/\partial\hat{t},-\hat{\mathbf{V}}\cdot\hat{\nabla})\mathbf{f}_\sigma^{(q)}-\sum_{p+q+r+2s=k+2}\hat{\mathbf{A}}_*(-\partial/\partial\hat{t})^s\mathbf{f}_*^{e2}[\rho_\sigma^{(p)},\hat{\mathbf{u}}_\sigma^{(q)},\hat{\mathbf{u}}_\sigma^{(r)}]=\hat{\mathbf{A}}_*\mathbf{f}_*^{e0}[\rho_\sigma^{(k+2)}]+\hat{\mathbf{A}}_*\sum_{p+q=k+2}\mathbf{f}_*^{e1}[\rho_\sigma^{(p)},\hat{\mathbf{u}}_\sigma^{(q)}]-\hat{\mathbf{A}}_*\mathbf{f}_\sigma^{(k+2)}+\hat{\mathbf{A}}_*\mathbf{k}^{(k+2)} \tag{110}$$

or, explicitly,

$$\mathbf{f}_\sigma^{(k+2)}=\sum_{p+q+r+2s=k+2}(-\partial/\partial\hat{t})^s\mathbf{f}_*^{e2}[\rho_\sigma^{(p)},\hat{\mathbf{u}}_\sigma^{(q)},\hat{\mathbf{u}}_\sigma^{(r)}]+\mathbf{f}_*^{e0}[\rho_\sigma^{(k+2)}]+\sum_{p+q=k+2}\mathbf{f}_*^{e1}[\rho_\sigma^{(p)},\hat{\mathbf{u}}_\sigma^{(q)}]+\hat{\mathbf{A}}_*^{\dagger}\sum_{p+q=k+2}D_p(-\partial/\partial\hat{t},-\hat{\mathbf{V}}\cdot\hat{\nabla})\mathbf{f}_\sigma^{(q)}+\mathbf{k}^{(k+2)}, \tag{111}$$

where

$$\mathbf{k}^{(k+2)}=-m\sum_{p+q=k+2}\{\mathbf{f}_\sigma^{e1}[\rho_\sigma^{(p)},\hat{\mathbf{u}}_\sigma^{(q)}]-\mathbf{f}_*^{e1}[\rho_\sigma^{(p)},\hat{\mathbf{u}}_\sigma^{(q)}]\}. \tag{112}$$

Equation (111) describes how the generic expansion coefficient $\mathbf{f}_\sigma^{(k+2)}$ depends on the actual values of the macroscopic moments and their time and space derivatives.

Since we are interested in recovering the macroscopic equations for the hydrodynamic conserved moments, it is useful to consider the equivalent formulation in the moment space, involving the expansion coefficients of the moments, given by

$$-\sum_{p+q=k+2}\mathbf{M}_A D_p(-\partial/\partial\hat{t},-\hat{\mathbf{V}}\cdot\hat{\nabla})\mathbf{f}_\sigma^{(q)}=\hat{\mathbf{E}}_*\mathbf{m}_*^{e0}[\rho_\sigma^{(k+2)}]+\hat{\mathbf{E}}_*\sum_{p+q=k+2}\mathbf{m}_*^{e1}[\rho_\sigma^{(p)},\hat{\mathbf{u}}_\sigma^{(q)}]+\hat{\mathbf{E}}_*\sum_{p+q+r+2s=k+2}(-\partial/\partial\hat{t})^s\mathbf{m}_*^{e2}[\rho_\sigma^{(p)},\hat{\mathbf{u}}_\sigma^{(q)},\hat{\mathbf{u}}_\sigma^{(r)}]-\hat{\mathbf{E}}_*\mathbf{m}_\sigma^{(k+2)}+\mathbf{M}_A\hat{\mathbf{A}}_*\mathbf{k}^{(k+2)}. \tag{113}$$

In particular we are interested in the lower-order expansion coefficients for the hydrodynamic moments only. For $k=0,+2$, the effects to the continuity equation are recovered:

$$\frac{\partial\rho_\sigma^{(0)}}{\partial\hat{t}}+\hat{\mathbf{V}}\cdot[\rho_\sigma^{(0)}\hat{\mathbf{u}}_\sigma^{(1)}]-\frac{s_\sigma}{6}\hat{\nabla}^2\rho_\sigma^{(0)}=0, \tag{114}$$

$$\frac{\partial\rho_\sigma^{(2)}}{\partial\hat{t}}+\hat{\mathbf{V}}\cdot\hat{\mathbf{j}}_\sigma^{(3)}-\frac{s_\sigma}{6}\hat{\nabla}^2\rho_\sigma^{(2)}-1\oplus[D_3(-\partial/\partial\hat{t},-\hat{\mathbf{V}}\cdot\hat{\nabla})\mathbf{f}_\sigma^{(1)}+D_4(-\partial/\partial\hat{t},-\hat{\mathbf{V}}\cdot\hat{\nabla})\mathbf{f}_\sigma^{(0)}]=0, \tag{115}$$

Similarly the effects to the momentum equation for $k=-1,+1$ are recovered:

$$s_\sigma/3\hat{\nabla}\rho_\sigma^{(0)}=-(1+m)\hat{\lambda}_m^I\rho_\sigma^{(0)}\hat{\mathbf{w}}_\sigma^{(1)}, \tag{116}$$

$$\hat{\nabla}\cdot\hat{\mathbf{T}}_\sigma^{(2)}-\hat{\mathbf{V}}\oplus[D_2(-\partial/\partial\hat{t},-\hat{\mathbf{V}}\cdot\hat{\nabla})\mathbf{f}_\sigma^{(1)}+D_3(-\partial/\partial\hat{t},-\hat{\mathbf{V}}\cdot\hat{\nabla})\mathbf{f}_\sigma^{(0)}]=\hat{\lambda}_m^I[\hat{\mathbf{j}}^{(3)}-\hat{\mathbf{j}}_\sigma^{(3)}]+\hat{\lambda}_m^I\hat{\mathbf{V}}\oplus\mathbf{k}^{(3)}. \tag{117}$$

After some simple algebra, the final form of Eq. (117) yields

$$\frac{\partial}{\partial\hat{t}}[\rho_\sigma^{(0)}\hat{\mathbf{u}}_\sigma^{(1)}]+\hat{\nabla}\cdot\hat{\mathbf{T}}_\sigma^{(2)}-\hat{\nabla}\cdot\left\{\frac{1}{2}\hat{\mathbf{V}}\oplus\hat{\mathbf{V}}\oplus[\hat{\mathbf{V}}\cdot\hat{\nabla}\mathbf{f}_\sigma^{(1)}]+\hat{\mathbf{V}}\oplus\hat{\mathbf{V}}\oplus\frac{\partial\mathbf{f}_\sigma^{(0)}}{\partial\hat{t}}-\frac{1}{6}\hat{\mathbf{V}}\oplus\hat{\mathbf{V}}\oplus[\hat{\mathbf{V}}\cdot\hat{\nabla}(\hat{\mathbf{V}}\cdot\hat{\nabla}\mathbf{f}_\sigma^{(0)})]\right\}=\hat{\lambda}_m^I[\hat{\mathbf{j}}^{(3)}-\hat{\mathbf{j}}_\sigma^{(3)}]+\hat{\lambda}_m^I\hat{\mathbf{V}}\oplus\mathbf{k}^{(3)}. \tag{118}$$

If the discrete scheme is compared with the continuous model, the first obvious result is that the same zeroth-order expansion coefficient $\mathbf{f}_\sigma^{(0)}$ is recovered. Even though it is less obvious, the same conclusion still holds for the first-order expansion coefficient $\mathbf{f}_\sigma^{(1)}$. It is easy to recover the latter result

by recalling the general equation (111) for the case $k=-1$—namely,

$$\mathbf{f}_{\sigma}^{(1)} = 3\rho_{\sigma}^{(0)}\hat{\mathbf{V}}\cdot[\mathbf{s}_I \otimes \hat{\mathbf{u}}_{\sigma}^{(1)}] - 3\frac{\hat{\lambda}_m^I}{s_\sigma}\hat{\mathbf{A}}_*^{\dagger}\hat{\mathbf{V}}\cdot[\mathbf{s}_0 \otimes \hat{\mathbf{b}}^{(1)}] + \mathbf{k}^{(1)}, \tag{119}$$

which after some algebra yields

$$\mathbf{f}_{\sigma}^{(1)} = \rho_{\sigma}\mathbf{M}_A^{-1}[0,\hat{u}_{\sigma x},\hat{u}_{\sigma y},0,0,0,0,0,0]^T. \tag{120}$$

This means that the artificial forcing term introduced by the first correction needed to derive the SILBE scheme does not effect the first-order expansion coefficient $\mathbf{f}_{\sigma}^{(1)}$. The additional forcing term produces a direct effect in the momentum equation, but it does not modify the dynamics of the first-order expansion coefficient. However, this direct effect in the momentum equation will be used to improve the accuracy of the scheme with regards to the continuity equation. In order to achieve this goal, the single species velocity must be redefined (this is the *second correction*)—namely,

$$\hat{\mathbf{u}}_{\sigma}^{*} = \hat{\mathbf{u}}_{\sigma} + n\hat{\mathbf{w}}_{\sigma}, \tag{121}$$

where n is a tunable parameter. It is easy to verify that independently of the value of the parameter n, the barycentric velocity does not need to be redefined—namely, $\hat{\mathbf{u}}^{*}=\hat{\mathbf{u}}$. Introducing the previous expression in Eqs. (114) and (119) yields

$$\frac{\partial\rho_{\sigma}^{(0)}}{\partial\hat{t}} + \hat{\boldsymbol{\nabla}}\cdot\left\{\rho_{\sigma}^{(0)}\hat{\mathbf{u}}_{\sigma}^{*(1)} + \rho_{\sigma}^{(0)}\hat{\mathbf{w}}_{\sigma}^{*(1)}\left[\frac{\hat{\lambda}_m^I}{2}\left(\frac{1+m}{1+n}\right) - \frac{n}{1+n}\right]\right\} = 0, \tag{122}$$

$$s_\sigma/3\hat{\boldsymbol{\nabla}}\rho_{\sigma}^{(0)} = -\hat{\lambda}_m^I\rho_{\sigma}^{(0)}\left(\frac{1+m}{1+n}\right)\hat{\mathbf{w}}_{\sigma}^{*(1)}. \tag{123}$$

Tuning $n=m=\hat{\lambda}_m^I/(2-\hat{\lambda}_m^I)$ yields

$$\frac{\partial\rho_{\sigma}^{(0)}}{\partial\hat{t}} + \hat{\boldsymbol{\nabla}}\cdot[\rho_{\sigma}^{(0)}\hat{\mathbf{u}}_{\sigma}^{*(1)}] = 0, \tag{124}$$

$$s_\sigma/3\hat{\boldsymbol{\nabla}}\rho_{\sigma}^{(0)} = -\hat{\lambda}_m^I\rho_{\sigma}^{(0)}\hat{\mathbf{w}}_{\sigma}^{*(1)}. \tag{125}$$

Combining the first and second corrections, the SILBE scheme allows one to solve the continuity equation and the diffusion equation without increasing the computational demand. In particular the distinct species flow velocity can be redefined during the post processing. Coherently with the common practice widespread in the lattice Boltzmann framework, this numerical trick allows one to correct the effects of a systematic error, which is clearly pointed out by the asymptotic analysis, by designing a properly modified scheme.

Concerning the second-order expansion coefficient $\mathbf{f}_{\sigma d}^{(2)}$, the discrete scheme departs from the results derived for the continuous model—namely,

$$\mathbf{f}_{\sigma d}^{(2)} = \rho_{\sigma}^{(2)}\mathbf{s}_I + \mathbf{f}_*^{e2}[\rho_{\sigma}^{(0)},\hat{\mathbf{u}}_{\sigma}^{(1)},\hat{\mathbf{u}}_{\sigma}^{(1)}] - \hat{\mathbf{A}}_*^{\dagger}\left\{\frac{\partial\mathbf{f}_{\sigma}^{(0)}}{\partial\hat{t}} + \hat{\mathbf{V}}\cdot[\hat{\boldsymbol{\nabla}}\mathbf{f}_{\sigma}^{(1)}] - \frac{1}{2}\hat{\mathbf{V}}\cdot\hat{\boldsymbol{\nabla}}[\hat{\mathbf{V}}\cdot\hat{\boldsymbol{\nabla}}\mathbf{f}_{\sigma}^{(0)}]\right\}. \tag{126}$$

Introducing the previous expansion coefficient in Eq. (118) yields

$$\begin{aligned}\frac{\partial}{\partial\hat{t}}[\rho_{\sigma}^{(0)}\hat{\mathbf{u}}_{\sigma}^{(1)}] + \hat{\boldsymbol{\nabla}}\cdot[\rho_{\sigma}^{(0)}\hat{\mathbf{u}}^{(1)}\otimes\hat{\mathbf{u}}^{(1)}] + s_\sigma/3\hat{\boldsymbol{\nabla}}\rho_{\sigma}^{(2)} &= \hat{\lambda}_m^I[\hat{\mathbf{j}}^{(3)} - \hat{\mathbf{j}}_{\sigma}^{(3)}] + \hat{\lambda}_m^I\hat{\mathbf{V}}\oplus\mathbf{k}^{(3)} + \hat{\boldsymbol{\nabla}}\cdot\left\{\hat{\mathbf{V}}\oplus\hat{\mathbf{V}}\oplus\left(\hat{\mathbf{A}}_*^{\dagger}+\frac{1}{2}\mathbf{I}\right)\right.\\ &\times\hat{\mathbf{V}}\cdot\hat{\boldsymbol{\nabla}}\mathbf{f}_{\sigma}^{(1)} + \hat{\mathbf{V}}\oplus\hat{\mathbf{V}}\oplus(\hat{\mathbf{A}}_*^{\dagger}+\mathbf{I})\frac{\partial\mathbf{f}_{\sigma}^{(0)}}{\partial\hat{t}}\\ &\left.-\frac{1}{2}\hat{\mathbf{V}}\oplus\hat{\mathbf{V}}\oplus\left(\hat{\mathbf{A}}_*^{\dagger}+\frac{1}{3}\mathbf{I}\right)[\hat{\mathbf{V}}\cdot\hat{\boldsymbol{\nabla}}(\hat{\mathbf{V}}\cdot\hat{\boldsymbol{\nabla}}\mathbf{f}_{\sigma}^{(0)})]\right\}.\end{aligned} \tag{127}$$

After some simple algebra, the final expression for the distinct species momentum equation is recovered:

$$\begin{aligned}\frac{\partial}{\partial\hat{t}}[\rho_{\sigma}^{(0)}\hat{\mathbf{u}}_{\sigma}^{(1)}] + \hat{\boldsymbol{\nabla}}\cdot[\rho_{\sigma}^{(0)}\hat{\mathbf{u}}^{(1)}\otimes\hat{\mathbf{u}}^{(1)}] + s_\sigma/3\hat{\boldsymbol{\nabla}}\rho_{\sigma}^{(2)} &= \hat{\lambda}_m^I[\hat{\mathbf{j}}^{(3)} - \hat{\mathbf{j}}_{\sigma}^{(3)}] + \hat{\lambda}_m^I\hat{\mathbf{V}}\oplus\mathbf{k}^{(3)}\\ &+\hat{\boldsymbol{\nabla}}\cdot\left\{\hat{\nu}_{md}[\hat{\boldsymbol{\nabla}}(\rho_{\sigma}^{(0)}\hat{\mathbf{u}}_{\sigma}^{(1)}t) + \hat{\boldsymbol{\nabla}}(\rho_{\sigma}^{(0)}\hat{\mathbf{u}}_{\sigma}^{(1)})^T]\right.\\ &+\hat{\eta}_{md}[\hat{\boldsymbol{\nabla}}\cdot\rho_{\sigma}^{(0)}\hat{\mathbf{u}}_{\sigma}^{(1)}]\mathbf{I} + \frac{1}{6}\left[\frac{s_\sigma}{3\hat{\lambda}_{m1}^{II}} - \frac{s_\sigma(2-s_\sigma)}{3\hat{\lambda}_{m3}^{II}}\right.\\ &\left.\left.+\frac{s_\sigma(3s_\sigma-1)}{9}\right]\hat{\boldsymbol{\nabla}}^2\rho_{\sigma}^{(0)}\mathbf{I} - \left(\frac{s_\sigma}{9\hat{\lambda}_{m1}^{II}} + \frac{s_\sigma}{18}\right)\hat{\boldsymbol{\nabla}}\hat{\boldsymbol{\nabla}}\rho_{\sigma}^{(0)}\right\},\end{aligned} \tag{128}$$

where $\hat{\nu}_{md}$ and $\hat{\eta}_{md}$ are defined as

$$\hat{\nu}_{md} = \frac{1}{3\hat{\lambda}_{m1}^{II}} + \frac{1}{6}, \tag{129}$$

$$\hat{\eta}_{md} = \frac{2-s_\sigma}{3\hat{\lambda}_{m3}^{II}} - \frac{1}{3\hat{\lambda}_{m1}^{II}} - \frac{2s_\sigma-1}{6}. \tag{130}$$

Concerning the distinct species momentum equation, the discrete formula implies some inconsistent terms which reduce the accuracy of the scheme up to the first order in space only. In this case, it is not easy to improve the performances of the scheme by designing some proper corrections. Fortunately in many applications first-order accuracy in space for solving the distinct species momentum is enough, as pointed out discussing the diffusion phenomenological equation given by Eq. (5), and it is coherent with the *single-fluid* approach (which completely neglects higher-order effects).

Moreover, if the relaxation frequencies are properly selected, it is possible to increase the accuracy in solving the barycentric momentum equation. In particular, if the relax-

ation frequencies controlling the bulk viscosities are selected in such a way to satisfy the condition

$$\frac{1}{\hat{\lambda}_{m3}^{II}} = \frac{3}{2-s_\sigma}\left(\hat{\eta}_m + \frac{1}{3\hat{\lambda}_{m1}^{II}} + \frac{2s_\sigma - 1}{6}\right), \tag{131}$$

then summing over the species yields

$$\begin{aligned}\frac{\partial}{\partial \hat{t}}[\rho^{(0)}\hat{\mathbf{u}}^{(1)}] + \hat{\boldsymbol{\nabla}}\cdot[\rho^{(0)}\hat{\mathbf{u}}^{(1)}\otimes\hat{\mathbf{u}}^{(1)}] \\ = -\hat{\boldsymbol{\nabla}}\hat{p}^{(2)}\hat{\boldsymbol{\nabla}}\cdot\{\hat{\nu}_{md}[\hat{\boldsymbol{\nabla}}(\rho^{(0)}\hat{\mathbf{u}}^{(1)}) + \hat{\boldsymbol{\nabla}}(\rho^{(0)}\hat{\mathbf{u}}^{(1)})^T] \\ + \hat{\eta}_{md}\hat{\boldsymbol{\nabla}}\cdot[\rho^{(0)}\hat{\mathbf{u}}^{(1)}]\mathbf{I}\},\end{aligned} \tag{132}$$

where $\hat{p}^{(2)}=\Sigma_\sigma s_\sigma \rho_\sigma^{(2)}/3$. The condition given by Eq. (131) was used to simplify some of the additional terms in Eq. (128) involving the density gradient.

Coming back to the original quantities expressed in physical units, it is easy to verify that $\tilde{\rho}_\sigma=\rho_\sigma^{(0)}$ and $\tilde{\mathbf{u}}_\sigma=\epsilon\mathbf{u}_\sigma^{*(1)}$ satisfy the continuity equation and the diffusion equation if terms $O(\epsilon^2)$ are neglected, while $\tilde{\rho}=\rho^{(0)}+\epsilon^2\rho^{(2)}$ and $\tilde{\mathbf{u}}=\epsilon\mathbf{u}^{(1)}$ satisfy the Navier-Stokes system of equations if terms $O(\epsilon^3)$ are neglected. In other words, the proposed scheme allows one to compute the mixture quantities with second-order accuracy by redefining the numerical viscosity, while introducing a fictitious forcing term and redefining the species velocity allow one to compute the distinct species quantities with first-order accuracy.

Some final remarks concerning the SILBE scheme are reported. The SILBE scheme is essentially a modified implicit formulation of the Euler integration rule. The scheme is completely *local* and it is very *stable* for a wide range of relaxation frequencies. The nonlinear terms in the equilibrium distribution function (according to the proposed semi-implicit-linearized approach) are computed explicitly. The asymptotic analysis discussed in this section proves that the previous approximations simplify the numerical implementation of the proposed scheme without effecting the desired accuracy. In order to solve the distinct species quantities with *first-order accuracy* in space, an additional forcing term (*first correction*) and a proper redefinition of the distinct species flow velocity (*second correction*) were considered. On the other hand, redefining the viscosities is enough for recovering the Navier-Stokes set of equations for the mixture with *second-order accuracy* in space, according to the common practice.

In the next section, some numerical results concerning the discussed schemes will be reported.

V. NUMERICAL RESULTS FOR SOME TEST CASES

A. Stability analysis by eigenvalue spectra for single-step integration formulas

First of all, the numerical stability of the single-step integration formulas for simple diffusion phenomena by means of von Neumann technique is reported. In the von Neumann analysis, the solution of the finite difference equation is written as the familiar Fourier series and the numerical stability is evaluated by the magnitude of eigenvalues of an amplification matrix [58].

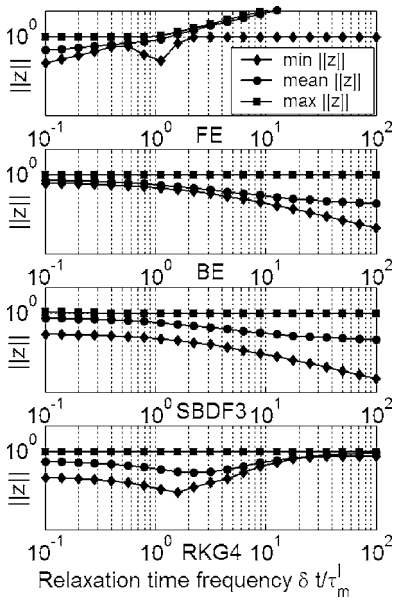

FIG. 1. Numerical results for the von Neumann stability analysis of single-step integration formulas. The minimum, maximum, and averaged moduli of the whole set of complex eigenvalues are reported for some values of the tunable relaxation frequency $\hat{\lambda}_m^I=\delta t/\tau_m^I \in [0.1,100]$. The following numerical schemes were considered: forward Euler (FE), backward Euler (BE), simplified backward differentiation formula with third-order accuracy (SBDF3), and finally the Runge-Kutta-Gauss formula with fourth-order accuracy (RKG4).

Even though this is not the only possible choice, in the following only the single-step integration formulas will be considered for the stability analysis, because in this case the identification of the amplification matrix is immediate. Moreover, the total pressure gradient acting on the mixture will be considered small and the external force will be neglected. These hypotheses allow one to consider the barycentric velocity small enough to be negligible, and consequently the dynamics of the distinct species is decoupled. In this way, the set of ordinary differential equations governing the phenomenon is given by Eq. (94), where $\bar{\mathbf{M}}_A$ depends on the considered integration formula. Finally, for simplifying the management of the dimensionless relaxation frequencies, they were selected in such a way that $\hat{\lambda}_\sigma^k=1$ for any $k\geqslant 2$ concerning the self-collisions and $\hat{\lambda}_m^k=\hat{\lambda}_m^I$ for any $k\geqslant 1$ concerning the cross collisions.

In the results of the numerical simulations reported in Fig. 1, four single-step integration formulas were considered: forward Euler (FE), backward Euler (BE), simplified backward differentiation formula with third-order accuracy (SBDF3), and finally the Runge-Kutta-Gauss formula with fourth-order accuracy (RKG4). As far as the stability analysis is concerned, the results obtained for the BE formula still hold for the SILBE, since the core of both solvers is the same. In particular the minimum, maximum, and averaged moduli of the whole set of complex eigenvalues are

reported for some values of the tunable relaxation frequency $\hat{\lambda}_m^I = \delta t / \tau_m^I \in [0.1, 100]$.

The FE scheme is the common implementation of the lattice Boltzmann method. Since the stability range is reduced by the relaxation of self-collisions characterized by $\hat{\lambda}_\sigma^k = 1$ for $k \geqslant 2$, this scheme will diverge for $\hat{\lambda}_m^I \geqslant 1$. This is confirmed by the von Neumann stability analysis, because the maximum modulus of the complex eigenvalues will be greater than unit (positive amplification) for $\hat{\lambda}_m^I \geqslant 1$ and, once this threshold is surpassed, it increases linearly with this relaxation frequency.

On the other hand, the BE scheme shows a very stable behavior. For the considered range of the relaxation frequencies, the modulus of all the eigenvalues is always smaller than unity (negative amplification) and in particular the averaged modulus is located in between the maximum and minimum values. This is important because it means that the eigenvalue spectrum is not becoming denser close to the stability threshold. The same considerations hold for the SBDF3 scheme.

The RKG4 scheme is stable for the whole considered range but the eigenvalue spectrum is becoming denser close to the stability threshold (early instability). This is consistent with the general theory of the numerical methods, because the size of the instability region grows as the order of the method increases. This indirectly proves that the common practice, widespread in the lattice Boltzmann community, of improving the accuracy by redefining the macroscopic transport coefficients does not contract the stability region, unlike what happens if more accurate schemes are considered.

In the next subsection, the performances of single-step and multistep methods with regards to the actual consistency for a simple test case will be compared.

B. Decay of the sine-wave density profile

In this section, the goal is to verify that the actual diffusivity of the numerical schemes reproduces the expected analytical results.

The transient method [19] is a very popular method for measuring the effective numerical diffusivity. Since in the present paper we are generally dealing with particle mass ratio different from unity—i.e., $e_A \neq e_B$—the equation for the mass concentration is not as simple as the ideal Fick's law should prescribe. In order to avoid of including an additional term due to pressure diffusion according to Eq. (73), it is possible to combine directly Eq. (68) and the continuity equation—namely,

$$\frac{\partial \tilde{\rho}_\sigma}{\partial t} + \boldsymbol{\nabla} \cdot (\tilde{\rho}_\sigma \tilde{\mathbf{u}}) = D_\sigma \nabla^2 \tilde{\rho}_\sigma, \tag{133}$$

which involves the distinct species diffusivity D_σ. Let us consider a set of starting density fields for each species $\tilde{\rho}_\sigma(x,0)$ in such a way that $\Sigma_\sigma e_\sigma \tilde{\rho}_\sigma(x,0)$ is constant. This implies that the total pressure gradient for the mixture is zero. In general it is not possible to deduce from the previous statement that the barycentric velocity will be necessarily zero, because the local composition of the mixture can effect the relationship between the total pressure and the total density during the approaching to equilibrium. This concept will be better discussed in Sec. V D. However, let us suppose in the present case that barycentric velocity is zero—i.e., $\tilde{u}_x = 0$. In the case D_σ is a constant, a solution of the Eq. (133), describing a decaying sine-wave density profile, is given as

$$\tilde{\rho}_\sigma(x,t) = \tilde{\rho}_\sigma^0 + (\tilde{\rho}_\sigma' - \tilde{\rho}_\sigma^0)\exp(-k^2 D_\sigma t)\sin(kx), \tag{134}$$

where $\tilde{\rho}_\sigma^0$ is the averaged density of the σ species, $\tilde{\rho}_\sigma'$ is the maximum value of the initial perturbation applied to the density, and $k = 2\pi/L$ is the wave number of the perturbation. Since periodic boundary conditions were used, the ratio between the computational domain length along x axis and the wavelength was an integer. The numerical diffusivity can be measured (*transient method*) by considering the sine-wave maximum decay—namely,

$$D_\sigma^{MT} = \frac{1}{k^2 t} \ln\left\{ \frac{\tilde{\rho}_a[\pi/(2k), 0] - \tilde{\rho}_\sigma^0}{\tilde{\rho}_\sigma[\pi/(2k), t] - \tilde{\rho}_\sigma^0} \right\}. \tag{135}$$

Another way for instantaneously measuring the species diffusivity (*flux method*) is based on the diffusion equation given by Eq. (68)—namely,

$$D_\sigma^{MF} = -\frac{\tilde{\rho}_\sigma(\tilde{u}_{\sigma x} - \tilde{u}_x)}{\partial \tilde{\rho}_\sigma / \partial x}. \tag{136}$$

When the numerical implementations due to discrete formulas are considered, these two methods could be not equivalent, as can be easily checked by considering, for example, the BE and FE schemes, which both satisfy Eq. (68) but not the general diffusion equation (133). In particular, taking into account Eq. (114), the theoretical diffusivity expected by means of the transient method for the Euler-based methods could be effected by the first-order error (if any) in the continuity equation—namely,

$$D_\sigma^{TT} = D_\sigma^{TF}\left(1 + \frac{\zeta}{2}\right), \tag{137}$$

where $D_\sigma^{TF} = e_\sigma / \lambda_m^I = D_\sigma$ is the theoretical diffusivity expected by means of the flux method, $\zeta = -\hat{\lambda}_m^I$ for FE, $\zeta = +\hat{\lambda}_m^I$ for BE, and finally $\zeta = 0$ for SILBE (where the redefined velocity must be considered).

The numerical results reported in Fig. 2 confirm the expected theoretical values obtained by means of the asymptotic analysis. In particular both the BE (limited to $\hat{\lambda}_m^I \leqslant 1$ by the stability threshold) and FE schemes do not satisfy the continuity equation because $D_\sigma^{TT} \neq D_\sigma^{TF} = D_\sigma$: in particular $D_\sigma^{TT} < D_\sigma^{TF}$ for BE and $D_\sigma^{TT} > D_\sigma^{TF}$ for FE. The results are very good for both SBDF3 and RKG4, which correctly ensure the continuity equation. The important difference between the previous two schemes is that the RKG4 scheme is highly nonlocal, because it involves the values of all the cells for updating each one of them. On the other hand, the SBDF3 scheme produces essentially the same results but with a four-cell-wide computational rule, which is not ideal for parallel computing, but much more local than the previous one.

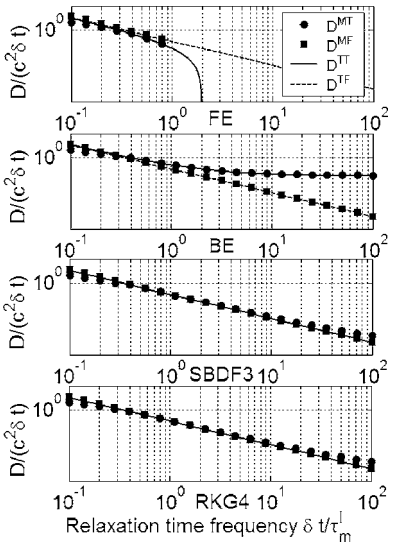

FIG. 2. Numerical results for the sine wave density decay (single-step formulas). The measured diffusivity obtained by means of the transient method D_σ^{MT} given by Eq. (135) and that obtained by means of the flux method D_σ^{MF} given by Eq. (136) are reported and compared with the corresponding theoretical values (D_σ^{TT} and D_σ^{TF}, respectively) given by Eq. (137). The reported numerical schemes are the same considered in Fig. 1.

For the decay of the sine-wave density profile, the multistep formulas (BDF2 and BDF3) do not seem to have any practical advantage. The numerical results concerning the multistep formulas are reported in Fig. 3. The results are as good as those obtained by the SBDF3 but with an additional memory demand, required by referring to the numerical solutions at the previous time steps. According to the asymptotic analysis, the BDF2 scheme is enough for correctly solving the continuity equation with second-order accuracy. The BDF3 is less robust for large values of the dimensionless relaxation frequency (in particular, the measured diffusivity for $\hat{\lambda}_m^I$ close to 100 tends to be negative). The fact that the numerical results diverge from those prescribed by

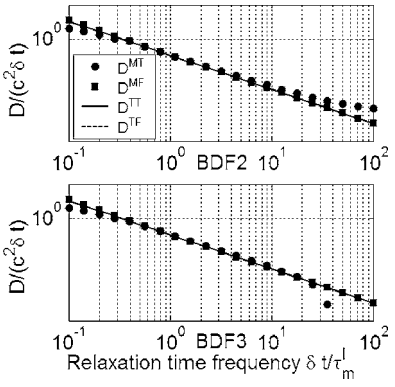

FIG. 3. Numerical results for the sine-wave density decay (multistep formulas). The involved parameters are the same considered in Fig. 2. The following numerical schemes were considered: backward differentiation formula with second-order accuracy (BDF2) and backward differentiation formula with third-order accuracy (BDF3).

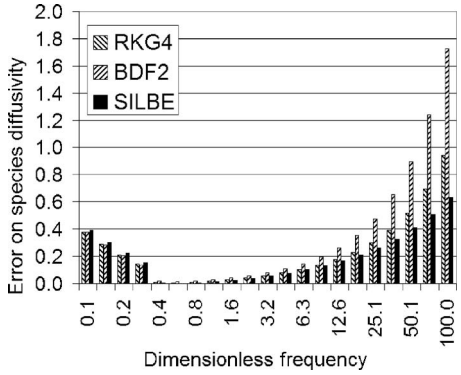

FIG. 4. Relative absolute error between the measured species diffusivity obtained by means of the *transient method* and the theoretical values. The following numerical schemes were considered: backward differentiation formula with second-order accuracy (BDF2), the Runge-Kutta-Gauss formula with fourth-order accuracy (RKG4), which produces performances analogous to the BDF3 scheme, and finally the semi-implicit-linearized backward Euler (SILBE) scheme.

the asymptotic analysis for large values of $\hat{\lambda}_m^I$ is reasonable because the assumed condition $O(\hat{\lambda}_m^I)=1$ does not hold any more. Again the stability performances are worst for more accurate schemes.

Finally the relative absolute error between the theoretical species diffusivity and the measured value obtained by means of the *transient method* (Fig. 4) and the *flux method* (Fig. 5) is reported. It is easy to verify that the corrections introduced for deriving the SILBE scheme are quite effective in recovering the desired set of macroscopic equations and, in particular, for solving the continuity equation with second-order accuracy. Moreover, these corrections do not contract the stability region of the scheme if compared to the original BE approach. In particular, the performances of the SILBE scheme for high values of $\hat{\lambda}_m^I$ are better than those of the RKG4.

The sine-wave density decay is a very simple test case, which essentially involves the continuity equation and the leading terms of the momentum equation only, which are the linear terms of the Navier-Stokes equations. Some doubts

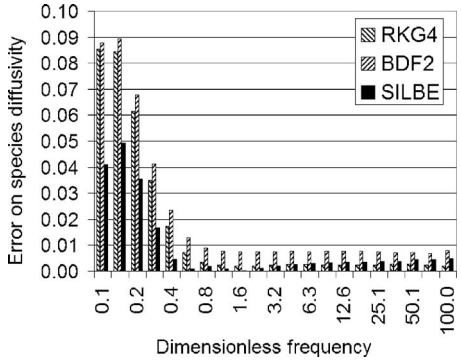

FIG. 5. Relative absolute error between the measured species diffusivity obtained by means of the *flux method* and theoretical values. The reported numerical schemes are the same considered in Fig. 4.

still remain concerning the fact that solving explicitly the nonlinear terms of the equilibrium distribution function could lead to instability. For this reason, in the next section the Taylor-Green vortex flow will be discussed.

C. Taylor-Green vortex flow

In order to check the effects due to solving explicitly the nonlinear terms in the equilibrium distribution function proposed in the framework of the semi-implicit-linearized schemes, the two-dimensional (2D) Taylor-Green vortex flow will be discussed as a test case. Let us consider an ideally decoupled mixture—i.e., a mixture defined in such a way that the cross collisions are negligible if compared with the self-collisions. In this case, each species will evolve according to an independent dynamics. We can imagine to initialize each species density in order to reproduce as many Taylor-Green vortex flows as the number of species. For simplifying the management of the dimensionless relaxation frequencies, they were selected in such a way that $\hat{\lambda}_\sigma^k=\hat{\lambda}_\sigma^{II}$ for any $k\geqslant 2$ concerning the self-collisions and $\hat{\lambda}_m^k=0$ for any $k\geqslant 1$ concerning the cross collisions.

In the low-Mach-number limit, the Taylor-Green vortex flow in two dimensions has the following analytic solutions to the incompressible Navier-Stokes equation:

$$\tilde{u}_{\sigma x}(x,y,t) = -U_0\cos(kx)\sin(ky)\exp(-2k^2\nu_\sigma t), \quad (138)$$

$$\tilde{u}_{\sigma y}(x,y,t) = +U_0\cos(ky)\sin(kx)\exp(-2k^2\nu_\sigma t), \quad (139)$$

$$\tilde{p}_\sigma(x,y,t) = -\frac{1}{4}U_0^2[\cos(2kx)+\cos(2ky)]\exp(-4k^2\nu_\sigma t) + P_{\sigma 0}, \quad (140)$$

where U_0 is the initial velocity amplitude, $k=2\pi/L$ is the wave number, and $P_{\sigma 0}$ is an arbitrary constant pressure (in the following $P_{\sigma 0}=0$ will be assumed). The (spatially) averaged total kinetic energy is

$$\langle E(t)\rangle = \frac{2}{L^2U_0^2}\int \tilde{\mathbf{u}}_\sigma^2(x,y,t)dxdy, \quad (141)$$

which should evolve in time as $\exp(-4k^2\nu_\sigma t)$. This suggests a practical way to measure the distinct species kinetic viscosity—namely,

$$\nu_\sigma^M = \frac{1}{4k^2t}\ln\left[\frac{\langle E(0)\rangle}{\langle E(t)\rangle}\right]. \quad (142)$$

It is easy to verify that the theoretical kinematic viscosity expected by means of the previous method could be effected by the second- and third-order errors due to the considered integration formula—namely,

$$\nu_\sigma^T = \frac{c^2}{3\lambda_\sigma^{II}}\left(1+\frac{\zeta}{2}\right), \quad (143)$$

where $\zeta=-\hat{\lambda}_\sigma^{II}$ for FE, $\zeta=+\hat{\lambda}_\sigma^{II}$ for both BE and SILBE (where the redefined velocity must be considered), and finally for $\zeta=0$ for the BDF3 scheme. Fortunately, according to the common practice, it is possible to improve the accuracy of the FE, BE, and SILBE schemes by redefining the actual kinematic viscosity. Unlike the species diffusivity, in this case redefining the kinematic viscosity is enough because the discretization error has exactly the same structure of the physical term we want to simulate.

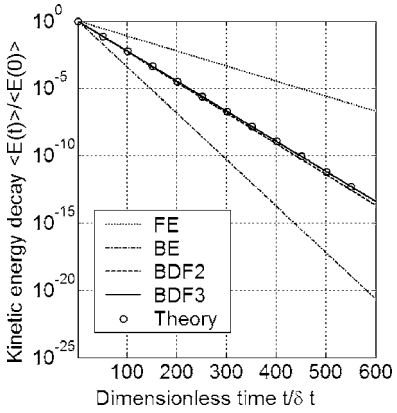

FIG. 6. Total kinetic energy decay in time for the Taylor-Green vortex flow ($\hat{\lambda}_\sigma^{II}=1$). The following numerical schemes were considered: forward Euler (FE), backward Euler (BE), equivalent in this test case to the SILBE scheme, backward differentiation formula with second-order accuracy (BDF2), and backward differentiation formula with third-order accuracy (BDF3).

The SBDF3 scheme, which was so promising according to the results for the sine wave density decay, completely fails for the present test case. In principle the SBDF3 scheme should move some steps towards the physical kinematic viscosity—namely, $\nu_\sigma^T=c^2/(3\lambda_\sigma^{II})$. In fact this scheme is characterized by the required spatial accuracy, even though the effects due to the errors in the estimation of the time derivatives should be better investigated by means of the asymptotic analysis. Unfortunately the scheme is not stable for the present case (this does not contradict the stability analysis performed previously, because it refers to a different test). The velocity field and consequently the total kinetic energy mimic the analytical solution during the first time steps, but cumulative errors in the pressure field force the scheme to diverge. This empirically proves that, generally speaking, moving along the lattice characteristics is a better strategy because it is closer to the physical meaning of the lattice representation.

In order to check the analytical expressions given by Eq. (143), in Fig. 6 some numerical results are reported. The numerical simulations confirm that the FE scheme underestimates, the BE-SILBE scheme overestimates, and finally the BDF2-BDF3 schemes closely reproduce the physical kinematic viscosity. Actually the performances of the BDF3 scheme are better than those obtained by means of the BDF2 scheme because the measured viscosity is closer to the physical one (as it is clear by carefully checking Fig. 6).

Finally in Fig. 7 some numerical results (the FE scheme is limited to $\hat{\lambda}_\sigma^{II}\leqslant 2$ by the stability threshold) concerning the measured kinematic viscosity for some values of the tunable relaxation frequency $\hat{\lambda}_\sigma^{II}=\delta t/\tau_\sigma^{II}\in[0.1,100]$ are reported. The numerical simulations are in good agreement with the predictions based on Eq. (143).

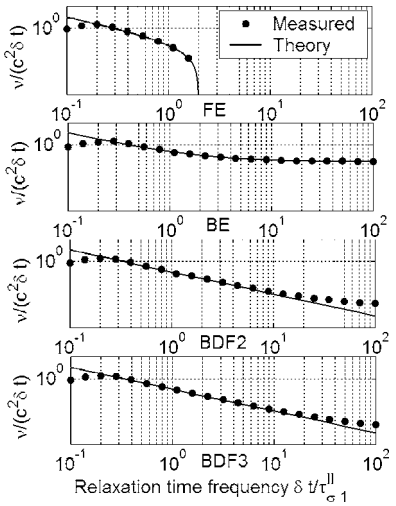

FIG. 7. Numerical results for the kinematic viscosity measured by means of the Taylor-Green vortex flow for some values of the tunable relaxation frequency $\hat{\lambda}_\sigma^{II}=\delta t/\tau_\sigma^{II}\in[0.1,100]$. The reported numerical schemes are the same considered in Fig. 6.

The previous numerical tests were preliminarily considered for checking the suggested numerical technique. In the next section, some additional tests are discussed, because they are more relevant for mixture modeling. In particular the case when the molecular weights of the two species of particles are different and the barycentric velocity becomes noticeable is analyzed.

D. Binary diffusion

In order to evaluate the advantages of the proposed model, two sets of computations are carried out. A proper binary mixture made of water and hydrogen is considered for dealing with a large particle mass ratio ($M_{H_2O}/M_{H_2}=9$). In the first case, the effects due to the barycentric velocity are neglected and this allows one to recover the results due to the Fick model in the macroscopic limit. Since this is not acceptable for this mixture, the dynamics of the barycentric velocity is taken into account in the second set of computations and consequently some results, which are consistent with the Maxwell-Stefan macroscopic model, are reported.

1. Fick macroscopic model

Let us consider hydrogen (A) and water (B) diffusing into each other at $T=1073$ K and $\tilde{p}^0=1\times10^5$ Pa, as total initial pressure. Consequently the total initial number density $\tilde{n}^0=\tilde{p}^0/(RT)=11.21$ mol/m^3, without distinguishing the nature of the particles.

As previously discussed, it is possible to deal with molecular weights of the two species, which are different from each other, by properly tuning the ratio between moving particles and those at rest—i.e., by means of s_σ. In this case, we selected to design the discrete numerical lattice in such a way so as to match the dynamics of the lighter (faster) particles—i.e., hydrogen—for which $s_A=1$. Consequently the dynamics of the heavier (slower) particles—i.e., water—must be corrected and this implies $s_B=1/9$. For this reason, the dimensionless energy for the species A can be expressed in lattice units as

$$\hat{e}_A=\frac{e_A}{c^2}=\frac{RT}{M_Ac^2}=\frac{1}{3}, \tag{144}$$

which implies $c=3658$ m/s. The lattice speed is the ratio between the discretization space step and the time step—namely, $c=\delta x/\delta t$—and, for this reason, high lattice velocities force one to reduce the corresponding time step and to increase the computational time. For this computation, the space step is $\delta x=0.25$ μm and consequently $\delta t=0.068$ ns.

The initial density profile for each species is assumed to have a hyperbolic tangent profile with the form [47]

$$\tilde{\rho}_A(x,t)=\tilde{\rho}_A^0\left[1+\tanh\left(\frac{x-L/2}{x_t}\right)\right], \tag{145}$$

$$\tilde{\rho}_B(x,t)=\tilde{\rho}_B^0\left[1-\tanh\left(\frac{x-L/2}{x_t}\right)\right], \tag{146}$$

where L is the length of the computational domain and x_t is the thickness of the diffusion profile. For this computation, $L=0.3$ mm and $x_t=\delta x=0.25$ μm (very sharp). This meas that the total number of discrete cells considered in these calculations is $L/\delta x=1200$. The maximum densities for both species are selected in such a way that $\tilde{\rho}_A^0/M_A=\tilde{\rho}_B^0/M_B=\tilde{n}^0/2$. In this way, it is easy to verify that $\tilde{n}(x,0)=\tilde{n}_A(x,0)+\tilde{n}_B(x,0)=\tilde{n}^0=\tilde{n}(x,t\to\infty)$; i.e., the total number of particles in each section is roughly constant and then consequently the total pressure is constant as well—i.e., $\tilde{p}(x,0)=\tilde{p}^0=\tilde{p}(x,t\to\infty)$. The selected numerical vales are $\tilde{\rho}_A^0=0.0112$ kg/m^3 and $\tilde{\rho}_B^0=0.1009$ kg/m^3.

On the other hand, the initial total density profile is

$$\tilde{\rho}(x,t)=\tilde{\rho}^0\left[1+\left(\frac{\tilde{\rho}_A^0-\tilde{\rho}_B^0}{\tilde{\rho}^0+\tilde{\rho}^0}\right)\tanh\left(\frac{x-L/2}{x_t}\right)\right], \tag{147}$$

which it is clearly not homogeneous in space. Recalling how the mutual diffusivity coefficient depends on the total density, namely,

$$D=\frac{RT\tilde{\rho}}{\lambda_m^I\tilde{n}M_AM_B}, \tag{148}$$

it is possible to update in each cell the relaxation parameter λ_m^I in such a way to recover the desired mutual diffusivity. At the considered temperature, the mutual diffusivity for the hydrogen-water binary mixture is $D=4.63$ cm^2/s [see Eq. (76)] and this values does not depend on the species concentrations. This means that the relaxation parameter λ_m^I should be tuned in each cell for compensating the spatial inhomogeneities due to $\tilde{\rho}$ in order to recover the desired value for D. Consequently the single-species diffusivity—i.e., $D_\sigma=e_\sigma/\lambda_m^I$—would be no more constant.

However, the final goal of the present calculations is to validate the model by proving that is allows one to catch consistently the dynamics of each species according to its molecular weight. It would be much more preferable to have fixed values for the single-species diffusivity D_σ,

because in this way it would easier to check the solutions of Eq. (133). For this reason, the average total density value—namely, $\tilde{\rho}^0=0.1121$ kg/m^3—has been used in the estimation of the relaxation parameter. This yields $\hat{\lambda}_m^I=0.3658$ and consequently $D_A=8.334$ cm^2/s for hydrogen and $D_B=0.926$ cm^2/s$\ll D_A$.

In this first set of calculations, the barycentric velocity has been neglected. This must not be considered a direct consequence of the fact that $\tilde{n}(x,0)=\tilde{n}^0=\tilde{n}(x,t\to\infty)$—i.e., of the fact that the total number density and the total pressure are roughly constant during the simulation. In fact the average molecular weight for the mixture, given by Eq. (71), varies spatially for compensating the spatial inhomogeneities due to the total density, as can be clearly proved by recalling that $\tilde{p}=RT(\tilde{\rho}/M)$. On the other hand, when steady equilibrium is approached, the species will have homogeneous concentrations over the computational domain and the mixture molecular weight would be homogeneous too, because in this case both the total pressure and the total density would be constant. This simple analysis proves that the total density must be characterized by some dynamics for passing from the initial configuration given by Eq. (147) to the final homogeneous configuration $\tilde{\rho}(x,t\to\infty)=\tilde{\rho}^0$. Finally, recalling the continuity equation, any time change in the density profile can only be achieved by some mass flux.

Despite the previous considerations, from the computational point of view it is always possible to neglect the barycentric velocity in the single-species dynamics by simply omitting the last coupling term in Eq. (102). For this reason, this kind of simulations can be defined as decoupled. In this case, the Eq. (133) reduces to

$$\frac{\partial\tilde{\rho}_\sigma}{\partial t}=D_\sigma\nabla^2\tilde{\rho}_\sigma. \tag{149}$$

The previous equation states that the equilibration process for water, with regards to both species density profile and partial pressure profile, will take a longer time than for hydrogen, because $D_B\ll D_A$. In Fig. 8 the species density profiles for the considered binary mixtures are reported at several times. In order to better clarify the different dynamics of the two species, the partial pressure profiles are reported in Fig. 9. It is evident from these pictures that the lighter particles (hydrogen) are characterized by a faster dynamics if compared to the heavier ones (water). This condition must be satisfied even though in the present calculations the initial partial pressure gradient for both species was the same—i.e., $\nabla\tilde{p}_A(x,0)=-\nabla\tilde{p}_B(x,0)$. This is a consequence of considering $D_B\ll D_A$. In fact, dividing Eq. (149) by the corresponding molecular weight and multiplying by RT, the equation governing the dynamics of the partial pressure $\tilde{p}_\sigma$ is recovered and it is easy to verify that the different dynamics between the two species is still preserved.

In the next paragraph, the effects due to the barycentric velocity will be discussed.

2. Maxwell-Stefan macroscopic model

First of all, we must discuss the order of magnitude of the corrections due to the barycentric velocity. Recalling that

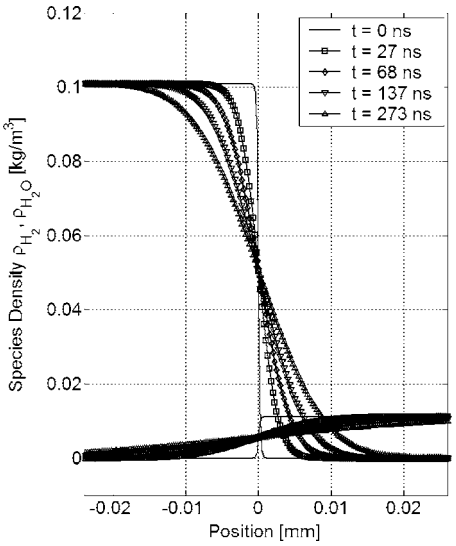

FIG. 8. Decaying density profiles for hydrogen (A on the right) and water (B on the left) at several times.

$\tilde{\mathbf{u}}_A-\tilde{\mathbf{u}}=x_B(\tilde{\mathbf{u}}_A-\tilde{\mathbf{u}}_B)$ and analogously $\tilde{\mathbf{u}}_B-\tilde{\mathbf{u}}=x_A(\tilde{\mathbf{u}}_B-\tilde{\mathbf{u}}_A)$, Eq. (69) yields

$$\tilde{\mathbf{u}}_A-\tilde{\mathbf{u}}_B=-\frac{\tilde{\rho}}{\tilde{\rho}_A\tilde{\rho}_B\lambda_m^I}\nabla\tilde{p}_A, \tag{150}$$

$$\tilde{\mathbf{u}}_B-\tilde{\mathbf{u}}_A=-\frac{\tilde{\rho}}{\tilde{\rho}_A\tilde{\rho}_B\lambda_m^I}\nabla\tilde{p}_B=-\frac{\tilde{\rho}}{\tilde{\rho}_A\tilde{\rho}_B\lambda_m^I}(\nabla\tilde{p}-\nabla\tilde{p}_A), \tag{151}$$

which means that it is possible to be consistent if and only if $O(|\nabla\tilde{p}|)\ll O(|\nabla\tilde{p}_A|)$. In other words, Eq. (69) considers only the leading term of Eq. (64), but it is usually enough for most of the diffusion phenomena. In fact, according to the asymptotic analysis, the previous condition is satisfied because $O(|\hat{\nabla}\hat{p}|)=\epsilon^3$ and $O(|\hat{\nabla}\hat{p}_A|)=\epsilon^1$. This means that the total pressure spatial gradients are smaller than those of the single species, but this does not imply that their effects are negligible.

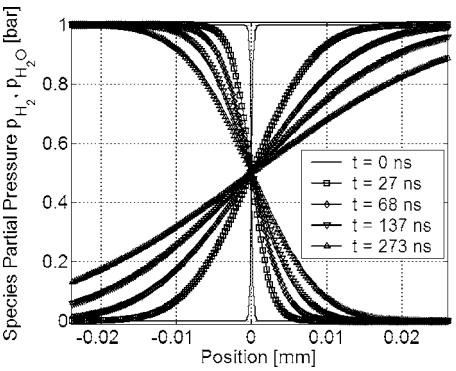

FIG. 9. Decaying partial pressure profiles for hydrogen (A on the right) and water (B on the left) at several times. It is evident from the picture that the lighter particles (hydrogen) are characterized by a faster dynamics, if compared to the heavier ones (water).

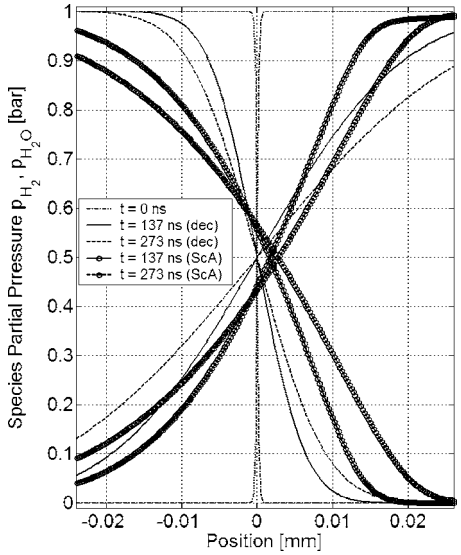

FIG. 10. Decaying partial pressure profiles for hydrogen (A on the right) and water (B on the left) at several times. The results obtained by taking into account the effects due to the barycentric velocity (Schmidt number $N_{\mathrm{Sc}_A}=0.6$) are compared with those obtained by neglecting it (decoupled simulation). Clearly the barycentric velocity induces a drag effect aiming to speed up the dynamics of water and to slow down the dynamics of hydrogen.

Let us introduce the effect of the barycentric dynamics ruled by the mixture viscosity. According to Eq. (79), the mixture kinematic viscosity depends on the local concentrations. Unfortunately this implies a varying Schmidt number, since $N_{\mathrm{Sc}}=\nu/D$. In the following calculations, the kinematic viscosity corresponding to the equilibrium homogeneous concentrations is assumed instead, in order to keep constant the Schmidt number. In particular, the mixture kinematic viscosity is 2.73 cm^2/s, which implies $\hat{\lambda}_{m1}^{II}=2.528$ and consequently $N_{\mathrm{Sc}}=0.6$.

The numerical results are reported in Fig. 10, and they are compared with the previous decoupled simulation. Clearly the barycentric velocity induces a drag effect aimed at speeding up the dynamics of water and to slow down the dynamics of hydrogen.

This is not the only effect due to the barycentric dynamics. If one looks closer at the density profiles for both species, it is possible to find some fast perturbations. An example of fast perturbation is reported in Fig. 11 at different times. The very sharp initial distribution of the total density given by Eq. (147) produces a perturbation, which effects the species density profiles as well, since they are now coupled each other. The perturbation propagates to the left in the flat water density profile. Actually the peak of this perturbation tends to become smoother coming along. It is easy to verify that the speed of these perturbations is $c/\sqrt{3}$, and so they can be considered pseudoacoustic waves (actually truly acoustic waves should be isoentropic instead of isothermal).

Finally, the effect of mixture kinematic viscosity on these perturbations is analyzed. The Schmidt number was doubled by considering a double kinematic viscosity. In particular, the artificial mixture kinematic viscosity is 5.46 cm^2/s, which implies $\hat{\lambda}_{m1}^{II}=0.7745$ and consequently $N_{\mathrm{Sc}}=1.2$. The

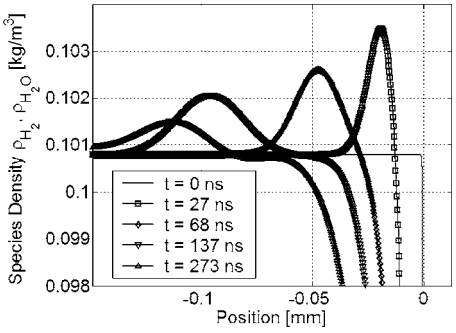

FIG. 11. Details concerning the decaying density profile of water at several times. The barycentric velocity is characterized by pseudoacoustic waves (actually truly acoustic waves should be isoentropic instead of isothermal), which effect the species density profiles as well.

numerical results are reported in Fig. 12. It is clear that doubling the value of the Schmidt number does not change significantly the perturbations. In particular the viscosity does not change the propagation time of the perturbation (confirming that it is an effect related to the pseudoacoustic damping) but only the overshooting.

In the next section, the main conclusions of this work will be summarized.

VI. CONCLUSIONS

The main conclusions of this paper are summarized in the following.

(A) A lattice Boltzmann model for mixture modeling has been developed by applying the multiple-relaxation-time approach to the Hamel model, which involves a simple model equation aiming to simplify the mixture modeling based on the continuous kinetic theory. The Hamel model allows one to derive from a general framework different model equations independently proposed, like (i) the Gross- Krook model [35], based on the linear relaxation of the actual distribution function to the equilibrium distribution function centered on the barycentric velocity, and (ii) and the Sirovich model [36], based on an additional forcing term proportional the diffusion velocity for modeling the coupling among the species due to cross collisions.

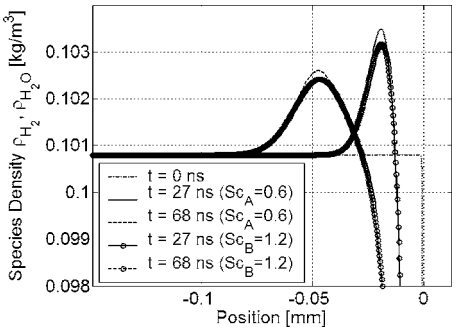

FIG. 12. Dependence of the perturbations in the water density profile induced by the pseudoacoustic waves on the Schmidt number ($N_{\mathrm{Sc}}=\nu/D$). It is clear that doubling the value of the Schmidt number does not change significantly the perturbations.

By imposing that (a) the pressure must be Galilean invariant and that (b) summing the nonlinear inertial tensor for each species must produce the same term for the mixture, the MRT lattice-Boltzmann Hamel model reduces to the generalized MRT lattice-Boltzmann Gross-Krook model, involving the local Maxwellian centered on the barycentric velocity only. However, the macroscopic transport coefficients—i.e., the species diffusivity, the mixture kinematic viscosity, and the mixture bulk viscosity—can still be independently tuned.

(B) Reducing the number of moving particles over the total—i.e., tuning $s_\sigma \leqslant 1$—is possible to effectively deal with mass particle ratios far from unity. In this way, the effects due to pressure-driven diffusion can be easily analyzed on the same computational lattice without any demanding interpolation. It is worth the effort to mention that this generalized equilibrium distribution function is consistent with the stability notion for lattice Boltzmann schemes recently suggested [60].

(C) Usually in the literature the concept of semi-implicit formulation is used for indicating lattice Boltzmann schemes which solve implicitly the collisional operator and explicitly the advection operator. This forces one to solve a (small) system of nonlinear equations for each computational cell during each time step. By means of the asymptotic analysis, it has been proved that it is possible to solve explicitly the nonlinear terms of the collisional operator without losing the wider stability typical of the implicit schemes. In this way, the calculations are drastically reduced and the operative matrices can be computed once for all, independently of the particular cell, at the beginning of the calculation.

(D) The elementary schemes based on the semi-implicit-linearized approach are not ideal for parallel computing because they involve more than one up-wind cell (or the full distribution function of the up-wind cell). For this reason, a modified backward Euler scheme, called the SILBE scheme, has been proposed. The key numerical tricks underlying the proposed scheme are (i) in order to solve the distinct species quantities with *first-order accuracy* in space, an additional forcing term (*first correction*) and a proper redefinition of the distinct species flow velocity (*second correction*) were considered; (ii) in order to solve the Navier-Stokes system of equations for the mixture with *second-order accuracy* in space, the viscosities were redefined, according to the common practice (simply taking into account a different sign for the discrete error due to the backward Euler formulation).

(E) For the considered application, the asymptotic analysis, recently suggested as an effective tool for analyzing the macroscopic equations corresponding to LB schemes, offers the possibility to easily deal with leading terms in the distribution functions, which are no longer Maxwellian. This represents a remarkable advantage in comparison with the classical Chapman-Enskog technique. On the other hand, these two techniques cannot be considered completely equivalent. The asymptotic analysis is based on a regular expansion of the distribution function which is suitable for the low Mach number limit—i.e., when the diffusive scaling applies (because diffusion prevails on advection). On the other hand, the Chapman-Enskog expansion is based on a multiscale expansion of the distribution function, which is suitable for describing phenomena with both advection (on the fast scale) and diffusion (on the slow scale). However, since the success of a multiscale expansion in correctly separating the scales is based on heuristic assumptions, it is better, whenever possible, to use a more rigorous regular expansion. For this reason, the reported results should be applied when the low-Mach-number assumption is acceptable.

(F) The numerical simulations confirm that the proposed model allows one to recover in the macroscopic limit both the Fick model (when the barycentric dynamics is neglected) and the Maxwell-Stefan model (when the barycentric dynamics is considered). The proposed model is perfectly suitable as far as the total density is smoothly varying in the computational domain (this is another way to require a low-Mach-number limit). If step-varying total density profiles are considered, some pseudoacoustic waves can emerge in the numerical results. Unfortunately, in this case, the numerical results cannot be considered reliable, because the diffusive scaling does not apply anymore and the intrinsic limits of the athermal lattice models appear (impossibility to recover isoentropic transformations).

ACKNOWLEDGMENTS

The author would like to sincerely thank Professor Michele Calì for his support and encouragement of this work. The author is very grateful to Professor Li-Shi Luo of the Old Dominion University for many enlightening discussions and for constantly sharing his results. Finally the author would like to thank Professor Taku Ohwada of the Kyoto University for helping him to understand the intrinsic limits of the simplified collision models.

[1] G. R. McNamara and G. Zanetti, Phys. Rev. Lett. **61**, 2332 (1988).
[2] F. Higuera, S. Succi, and R. Benzi, Europhys. Lett. **9**, 4 (1989).
[3] F. Higuera, J. Jimenez, and S. Succi, Europhys. Lett. **9**, 663 (1989).
[4] H. Chen, S. Chen, and W. H. Matthaeus, Phys. Rev. A **45**, R5339 (1992).
[5] Y. H. Qian, D. D'Humieres, and P. Lallemand, Europhys. Lett. **17**, 479 (1992).
[6] X. He and L.-S. Luo, Phys. Rev. E **56**, 6811 (1997).
[7] X. Shan and X. He, Phys. Rev. Lett. **80**, 65 (1998).
[8] M. G. Ancona, J. Comput. Phys. **115**, 107 (1994).
[9] D. Wolf-Gladrow, *Lattice-Gas Cellular Automata and Lattice Boltzmann Models*, Lecture Notes in Mathematics, Vol. 1725 (Springer-Verlag, Berlin, 2000).
[10] S. Succi, *The Lattice Boltzmann Equation for Fluid Dynamics and Beyond* (Oxford University Press, New York, 2001).

[11] G. D. Doolen, *Lattice Gas Methods for Partial Differential Equations* (Addison-Wesley, New York, 1990).
[12] R. Benzi, S. Succi, and M. Vergassola, Phys. Rep. **222**, 145 (1992).
[13] S. Chen and G. D. Doolen, Annu. Rev. Fluid Mech. **30**, 329 (1998).
[14] B. Manz, L. F. Gladden, and P. B. Warren, AIChE J. **45**, 1845 (1999).
[15] Th. Zeiser, P. Lammers, E. Klemm, Y. W. Li, J. Bernsdorf, and G. Brenner, Chem. Eng. Sci. **56**, 1697 (2001).
[16] K. Xu, J. Comput. Phys. **134**, 122 (1997).
[17] Y. S. Lian and K. Xu, J. Comput. Phys. **163**, 349 (2000).
[18] X. Shan and H. Chen, Phys. Rev. E **47**, 1815 (1993).
[19] E. G. Flekkoy, Phys. Rev. E **47**, 4247 (1993).
[20] X. Shan and G. Doolen, J. Stat. Phys. **81**, 379 (1995).
[21] X. Shan and G. Doolen, Phys. Rev. E **54**, 3614 (1996).
[22] E. Orlandini, W. R. Osborn, and J. M. Yeomans, Europhys. Lett. **32**, 463 (1995).
[23] W. R. Osborn, E. Orlandini, M. R. Swift, J. M. Yeomans, and J. R. Banavar, Phys. Rev. Lett. **75**, 4031 (1995).
[24] M. R. Swift, E. Orlandini, W. R. Osborn, and J. M. Yeomans, Phys. Rev. E **54**, 5041 (1996).
[25] A. Lamura, G. Gonnella, and J. M. Yeomans, Europhys. Lett. **45**, 314 (1999).
[26] V. Sofonea and R. F. Sekerka, Physica A **299**, 494 (2001).
[27] Z. Guo and T. S. Zhao, Phys. Rev. E **68**, 035302(R) (2003).
[28] L.-S. Luo and S. S. Girimaji, Phys. Rev. E **67**, 036302 (2003).
[29] A. Xu, Europhys. Lett. **69**, 214 (2005).
[30] P. C. Fancin, P. C. Philippi, and L. O. E. dos Santos, FGCS, Future Gener. Comput. Syst. **20**, 945 (2004).
[31] P. Asinari, Phys. Fluids **17**, 067102 (2005).
[32] B. B. Hamel, Ph.D. dissertation, Princeton University, 1963.
[33] B. B. Hamel, Phys. Fluids **8**, 418 (1965).
[34] B. B. Hamel, Phys. Fluids **9**, 12 (1966).
[35] E. P. Gross and M. Krook, Phys. Rev. **102**, 593 (1956).
[36] L. Sirovich, Phys. Fluids **5**, 908 (1962).
[37] D. d'Humiéres, in *Rarefied Gas Dynamics: Theory and Simulations*, edited by B. D. Shizgal & D. P. Weaver [Prog. Astronaut. Aeronaut. **159**, 450 (1992)].
[38] P. Lallemand and L.-S. Luo, Phys. Rev. E **61**, 6546 (2000).
[39] M. Junk and W.-A. Yong, Asymptotic Anal. **35**, 165185 (2003).
[40] M. Junk, A. Klar, and L.-S. Luo, J. Comput. Phys. **210**, 676 (2005).
[41] S. Harris, *An Introduction to the Theory of the Boltzmann Equation* (Holt Rinehart and Winston, New York, 1971).
[42] I. Ginzburg, Adv. Water Resour. **28**, 1171 (2005).
[43] C. Cercignani, *The Boltzmann Equation and its Application* (Springer, New York, 1988).
[44] Y. Sone, *Kinetic Theory and Fluid Dynamics* (Birkhäuser, Boston, 2002).
[45] S. Chapman and T. G. Cowling, *The Mathematical Theory of Non-Uniform Gases* (Cambridge University Press, Cambridge, England, 1970).
[46] R. C. Reid, *The Properties of Gases and Liquids* (McGraw-Hill, New York, 1987).
[47] M. E. McCracken and J. Abraham, Phys. Rev. E **71**, 046704 (2005).
[48] T. Lee and C. L. Lin, J. Comput. Phys. **185**, 445 (2003).
[49] J. Tolke, M. Krafczyk, M. Schulz, E. Rank, and R. Berrios, Int. J. Mod. Phys. C **9**, 1143 (1998).
[50] J. Tolke, M. Krafczyk, and E. Rank, J. Stat. Phys. **107**, 573, (2002).
[51] D. R. Noble, J. G. Georgiadis, and R. O. Buckius, Int. J. Numer. Methods Fluids **23**, 1 (1996).
[52] K. Sankaranarayanan, X. Shan, I. G. Kevrekidis, and S. Sundaresan, J. Fluid Mech. **452**, 61 (2002).
[53] R. R. Nourgaliev, T. N. Dinh, and B. R. Sehgal, Nucl. Eng. Des. **211**, 153 (2002).
[54] P. Szymczak and A. J. C. Ladd, Geophys. Res. Lett. **31**, L23606 (2004).
[55] T. Lee and C. L. Lin, Phys. Rev. E **71**, 046706 (2005).
[56] M. Bernaschi, S. Succi, H. D. Chen, and R. Y. Zhang, Int. J. Mod. Phys. C **13**, 675 (2002).
[57] M. Bernaschi and S. Succi, Int. J. Mod. Phys. B **17**, 1 (2003).
[58] T. Seta and R. Takahashi, J. Stat. Phys. **107**, 557 (2002).
[59] N. Z. Cao, S. Y. Shen, S. Jin, and D. Martinez, Phys. Rev. E **55**, R21 (1997).
[60] M. K. Banda, W.-A. Yong, and A. Klar, SIAM J. Sci. Comput. (USA), **27**(6), 2098 (2006).